Journal of Fluids and Structures (1998) **12,** 959–1003
Article. No. fl980179

VIBRO-ACOUSTIC BEHAVIOR OF SUBMERGED CYLINDRICAL SHELLS: ANALYTICAL FORMULATION AND NUMERICAL MODEL

F. Bérot and B. Peseux

Laboratoire de Mécanique et Matériaux, Division Mécanique des Structures,
Ecole Centrale de Nantes
BP 92101 - 44321, Nantes, France

(Received 26 May 1997 and in revised form 2 September 1998)

We propose both an analytical formulation and a numerical model to study the hydroelastic or vibroacoustic behaviour of cylindrical thin shells immersed in an unbounded, inviscid and heavy fluid. The analytical solution allows us to calculate the dynamic response and the pressure radiated in the far field by a baffled cylinder. This formulation uses the truncated modal basis of the dry structure to expand the displacements of the submerged shell. The analytical model is used as a reference in order to validate a numerical model which couples the finite element method (FEM) to the boundary element method (BEM). As opposed to the analytical formulation which is dedicated to baffled circular cylinders only, the numerical model allows us to treat any axisymmetric shell, such as cylindrical and spherical shells, or more complex shells of revolution. The structure is idealized by two-node ring finite elements and the boundary equation is solved using the method of singularities.

1. INTRODUCTION

For many years, numerous authors have been interested in the dynamic behaviour of thin cylindrical shells. We can mention, for example, the very good study realized by Leissa (1973) or the comparison between Donnell's theory, Flügge's theory and Sanders' theory made by Dym (1973) and also the last numerical work by Gonçalves & Ramos (1997). In the literature we can also find some papers concerning cylindrical shells with internal liquid, by Lakis & Païdoussis (1971, 1972), Lakis and Neagu (1997) Terhune & Karim-Panahi (1993), Mistry & Menezes (1995), for example. Concerning the dynamic behaviour of submerged thin cylindrical shells, most of the publications deal with the analytical approach to the vibro-acoustic behaviour of shells submerged in an unbounded fluid domain. In general, the analytical formulation of coupled problems has been made possible for some simple structures such as plates, beams, spheres and cylinders, and for some boundary conditions. Sandman (1976) presented an analytical formulation of a finite cylindrical shell closed by two rigid plates. Stephanishen (1982) and Laulagnet & Guyader (1989, 1990) proposed to evaluate the pressure field, the vibratory response and the radiated properties of a submerged finite cylinder with infinite rigid baffles connected to the shell. These authors show that the vibro-acoustic behaviour of a finite baffled shell is equivalent to the behaviour of a finite shell. Contrary to what happens in the dynamic behaviour of a dry shell, the modes of the immersed structure are coupled via the heavy fluid medium. Junger & Feit (1972)

0889–9746/98/080959 + 45 $30.00/0

proposed a solution for an infinite cylinder. In their model, the intermodal coupling induced by the outer fluid is neglected. Even in a heavy fluid, this simple solution gives the same resonant frequencies as the models proposed by Stephanishen and Laulagnet & Guyader. This analytical point of view is very useful in identifying the radiation properties of classical shapes. However, the analysis of complex shells requires other solutions (Grosh *et al.* 1994).

The power of numerical models enables us to study industrial structures for all kinds of boundary conditions (Morand & Ohayon 1995). Whereas the analytical formulations are obtained by discretization of the solution of the governing equations, the numerical solutions are defined as an idealization of the governing equations themselves. Nevertheless, if this second approach is more powerful than the analytical one, its development is limited by numerical problems such as by the large CPU time and large storage memory required. In this paper, we propose two kinds of solutions to study the vibro-acoustic behaviour of cylindrical shells: one analytical and the other numerical.

Firstly, the analytical formulation concerns a baffled circular thin cylindrical shell. We use a classical decomposition of the displacements of the immersed shell based on the modal basis of the finite dry shell. Unlike several other works (Sandman 1976; Stephanishen 1982; Laulagnet & Guyader 1989, 1990; Lesueur 1988) in which the fluid problem is treated by boundary integral equations, the pressure in the outer domain is established here using the governing equations only, Helmholtz's or Laplace's, and the boundary conditions on the shell and at infinity. We show that it is not advisable to neglect the cross-modal coupling in the calculation of the amplitudes of displacements of the immersed structure.

Next, we propose a numerical model which couples the finite element method to the boundary element method. With the aim of reducing storage memory problems inherent to this family of coupled models, we use a two-node ring finite element (Gould 1985; Percy *et al.* 1965) to model the shell of revolution. Thus, the thin shell is idealized into a series of conical frusta joining nodal circles. There are two families of ring finite elements: elements having a meridian curvature (Gould & Basu 1977; Grafton & Strome 1963) and conical elements. The numerical model presented in the second part of paper is a conical ring element. The simplicity of this element and its accuracy as a model of a simple curvature shell makes it suitable for the study of fluid–structure interactions.

2. ANALYTICAL FORMULATION

We consider a simply supported finite cylindrical shell connected to two infinite rigid baffles. This shell is assumed to be thin, isotropic and homogeneous and its geometrical parameters are: length L, mean radius R, constant thickness h and its mechanical characteristics: Young's modulus E, Poisson's ratio ν, and density ρ_s. The shell is immersed in an unbounded, inviscid, irrotational and compressible or incompressible fluid of density ρ_f. If the fluid is assumed to be compressible, the sound velocity is c.

A cylindrical coordinate system $(0, \mathbf{e}_r, \mathbf{e}_\theta, \mathbf{e}_z)$ is defined and the limits of the elastic shell are $z = 0$ and $z = L$ (Figure 1). The cylinder is excited by a time harmonic point driving force $\mathbf{F}$ applied to the mid-shell surface at $r = R$, $\theta = \theta_f$ and $z = z_f$:

$$\mathbf{F} = (f_u \mathbf{e}_r + f_v \mathbf{e}_\theta + f_w \mathbf{e}_z) \exp(-\mathrm{j}\omega t), \tag{1}$$

where

$$\begin{aligned} f_u &= \delta(z - z_f)\delta(\theta - \theta_f)\,\mathbf{F}\mathbf{e}_r, \\ f_v &= \delta(z - z_f)\delta(\theta - \theta_f)\,\mathbf{F}\mathbf{e}_\theta, \\ f_w &= \delta(z - z_f)\delta(\theta - \theta_f)\,\mathbf{F}\mathbf{e}_z; \end{aligned} \tag{2}$$

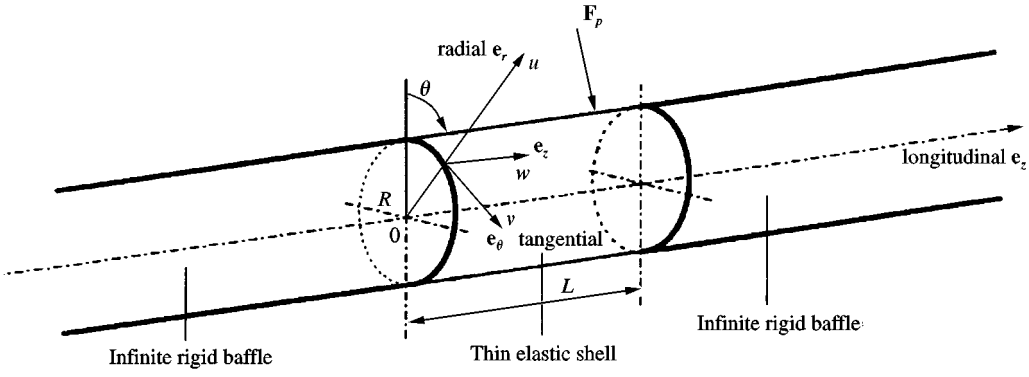

Figure 1. Coordinate system and dimensions of the cylindrical shell.

$\delta(\ )$ denotes the Dirac delta function. f_u, f_v, and f_w are the radial, tangential and longitudinal components of the driving force in the previous in the previous coordinate system.

2.1. Equation of Motion of a Dry Finite Cylinder

The elastic shell is considered with respect to the Kirchhoff–Love hypothesis. The matrix equation of motion for the free vibrations of a dry cylinder can be written as follows:

$$[K]\begin{Bmatrix} u \\ v \\ w \end{Bmatrix} + \rho_s h \begin{Bmatrix} \ddot{u} \\ \ddot{v} \\ \ddot{w} \end{Bmatrix} = \begin{Bmatrix} 0 \\ 0 \\ 0 \end{Bmatrix}, \tag{3}$$

where u, v and w are the displacement component of a point P on the mean surface; and $[K]$ is Donnell's or Flügge's operator (see Appendix A). Donnell's operator is obtained when the shell is assimilated to its mean surface. In this case, the thickness h is neglected compared to the mean radius R. Generally, Donnell's operator is preferred when h/R is small, whereas Flügge's operator can be used when h/R is larger. Solving this eighth-order system requires eight boundary conditions. In the classical case of a simply supported cylinder (Leissa 1973), the radial and tangential displacements, as well as bending moment M_{zz} and normal force N_z, are zero at the ends of the shell. Thus, the boundary conditions are $u = v = w_{,z} = u_{,zz} = 0$ at $z = 0$ and $z = L$. Considering these conditions, the separation of variables (space and time) is used to solve the equation of free vibrations. Hence, the displacement field is taken in the two following forms, symmetric or antisymmetric with respect to $\theta = 0$:

$$\begin{aligned} u &= U_0 \cos(n\theta)\sin(k_m z)\exp(-\mathrm{j}\omega t), & u &= U_0 \sin(n\theta)\sin(k_m z)\exp(-\mathrm{j}\omega t), \\ v &= V_0 \sin(n\theta)\sin(k_m z)\exp(-\mathrm{j}\omega t), \quad \text{or} & v &= V_0 \cos(n\theta)\sin(k_m z)\exp(-\mathrm{j}\omega t), \\ w &= W_0 \cos(n\theta)\cos(k_m z)\exp(-\mathrm{j}\omega t), & w &= W_0 \sin(n\theta)\cos(k_m z)\exp(-\mathrm{j}\omega t), \end{aligned} \tag{4}$$

with $k_m = m\pi/L$ and $n \in [0, +\infty]$, $m \in [1, +\infty]$. The parameters m and n are, respectively, the longitudinal and circumferential half-wavenumbers. In fact, if the displacement field is symmetric, substitution of the displacement field (4) into the governing equation of motion (3) finally leads to the following sixth-order equation:

$$\Omega^6 + K_1\Omega^4 + K_2\Omega^2 + K_3 = 0, \tag{5}$$

where Ω is the nondimensional circular frequency such that $\Omega^2 = \omega^2/\omega_a^2$, and $\omega_a^2 = E/[(1-\nu^2)\rho_s R^2]$ is the ring frequency. Thus,

$$\Omega^2 = \frac{(1-\nu^2)\rho_s R^2}{E}\omega^2. \tag{6}$$

where K_1, K_2, and K_3 are defined for both Flügge's and Donnell's theories in Appendix A.

The solution of equation (5) allows us to determine the natural frequencies of a dry, cylindrical, and simply supported thin shell. To each pair (m, n) correspond three double eigenvalues ω_i^2, $i = 1, 2, 3$:

$$\begin{aligned}
\omega_{mn1}^2 &= \omega_a^2\left(-\frac{2}{3}\sqrt{K_1^2 - 3K_2}\cos\left(\frac{\varphi}{3}\right) - \frac{K_1}{3}\right),\\
\omega_{mn2}^2 &= \omega_a^2\left(-\frac{2}{3}\sqrt{K_1^2 - 3K_2}\cos\left(\frac{\varphi + 2\pi}{3}\right) - \frac{K_1}{3}\right),\\
\omega_{mn3}^2 &= \omega_a^2\left(-\frac{2}{3}\sqrt{K_1^2 - 3K_2}\cos\left(\frac{\varphi + 4\pi}{3}\right) - \frac{K_1}{3}\right),
\end{aligned} \tag{7}$$

where φ is defined as

$$\varphi = \arccos\left(\frac{27K_3 + 2K_1^3 - 9K_1K_2}{2\sqrt{(K_1^2 - 3K_2)^3}}\right). \tag{8}$$

The subscript i denotes the three possible types of deformation: $i = 1$ corresponds to bending, $i = 2$ to torsion and $i = 3$ to extension–compression. These expressions for the frequencies are the same, irrespective of the mode of deformation being symmetric or antisymmetric. Usually, the case corresponding to the circumferential wavenumber $n = 0$ can be treated separately with separation of the axisymmetric problems (symmetric modes) and the torsional problems (antisymmetric models). Nevertheless, we keep here a general formulation and, finally, the frequencies ω_i and their associated mode shapes lead to the determination of the modal basis of the dry structure. We have

$$\begin{Bmatrix} u \\ v \\ w \end{Bmatrix} = \sum_{\delta=0}^{1}\sum_{n=0}^{\infty}\sum_{m=1}^{\infty}\sum_{i=1}^{3} a_{mni}^{\delta} \begin{Bmatrix} \sin k_m z \sin\left(n\theta + \delta\dfrac{\pi}{2}\right) \\ \dfrac{V_{0mni}}{U_{0mni}} \sin k_m z \cos\left(n\theta + \delta\dfrac{\pi}{2}\right) \\ \dfrac{W_{0mni}}{U_{0mni}} \cos k_m z \sin\left(n\theta + \delta\dfrac{\pi}{2}\right) \end{Bmatrix} g_{mni}(t); \tag{9}$$

δ indicates the antisymmetric ($\delta = 0$) or symmetric ($\delta = 1$) character of a shell mode with respect to $\theta = 0$. In this expression, there is a summation pertaining to symmetry (δ), one to each of the half-wavenumbers (m and n) and finally one to the type of deformation (i). a_{mni}^{δ} is the modal amplitude, $g_{mni}(t)$ is the time-dependent function expressed in terms of the modal circular eigenfrequencies ω_{mni}: $g_{mni}(t) = \exp(\omega_{mn}t)$, and $(1, V_{0mni}/U_{0mni}, W_{0mni}/U_{0mni})$ is the eigenvector shape of a shell mode when the first component U_{0mni} is normalized to unity. Thus,

$$\begin{aligned}
U_{0mni} &= 1,\\
V_{0mni} &= -U_{0mni}\frac{A_2(\Omega_{mni}^2 - C_3) - A_3C_2}{(\Omega_{mni}^2 - B_2)(\Omega_{mni}^2 - C_3) - B_3^2},\\
W_{0mni} &= -U_{0mni}\frac{A_3(\Omega_{mni}^2 - B_2) - B_3A_2}{(\Omega_{mni}^2 - B_2)(\Omega_{mni}^2 - C_3) - B_3^2}.
\end{aligned} \tag{10}$$

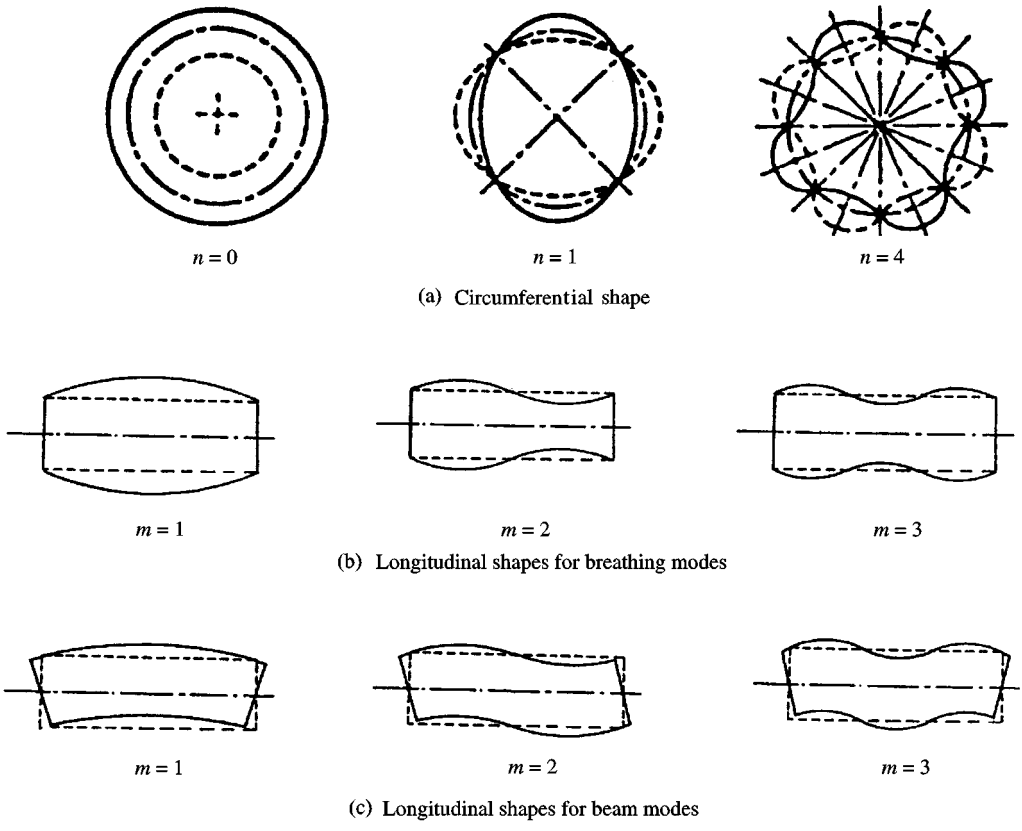

Figure 2. Mode shapes of a simply supported cylinder (Lindholm *et al.* 1962; Forsberg 1964; Leissa 1973).

These components are expressed as functions of the associated nondimensional eigenvalue Ω_{mni}, and the geometrical and mechanical characteristics of the elastic cylindrical shell. Figure 2 shows the different types of mode shapes that can occur in the study of the simply supported cylinder. The circumferential shapes are shown in Figure 2(a), the longitudinal breathing modes are shown in Figure 2(b) and the beam modes in Figure 2(c).

2.2. Governing Equations of the Compressible Fluid

We consider a pressure variation of the fluid about its equilibrium position. The irrotational motion of an inviscid and compressible fluid can be described by the velocity potential Φ. In the unbounded medium, the potential function Φ must satisfy Helmholtz's equation, Sommerfeld's radiation condition and the boundary condition on the fluid–structure interface. The appropriate boundary condition at the fluid–solid interface is the continuity of normal velocities. The elastic shell generates a radial movement of the outer fluid, but the velocity is zero on the baffles. This implies the following formulation for the fluid behaviour:

(i) the Helmholtz equation:

$$\Delta\Phi(r, \theta, z, t) - \frac{1}{c^2}\frac{\partial^2\Phi(r, \theta, z, t)}{\partial t^2} = 0; \tag{11}$$

defining the acoustic wavenumber, $k_f = \omega/c$, this leads to

$$\Delta\Phi + k_f^2\Phi = 0;$$

(ii) Sommerfeld's condition at infinity:

$$\lim_{r\to\infty} r\left(\frac{\partial\Phi}{\partial r} - k_f\Phi\right) = 0; \tag{12}$$

(iii) boundary conditions on the vibrating elastic structure, i.e. for $z \in [0, L]$:

$$\left.\frac{\partial\Phi(r,\theta,z,t)}{\partial r}\right|_{r=R} = \dot{u}(\theta,z,t); \tag{13}$$

(iv) boundary conditions on the rigid baffles, i.e. for $z \le 0$ and $z \ge L$

$$\left.\frac{\partial\Phi(r,\theta,z,t)}{\partial r}\right|_{r=R} = 0. \tag{14}$$

For the structure under study (elastic shell with infinite rigid baffles) the radial displacement u is not periodic in the axial direction. This lack of periodicity on the wall makes it impossible to solve the previous governing system in its basic form. It is therefore necessary to use the spatial Fourier transform of these equations along the z coordinate (Bérot 1997). With this view, we denote by $\tilde{\Phi}(r,\theta,\xi,t)$ the Fourier transform of $\Phi(r,\theta,z,t)$, and by $\tilde{\dot{u}}(\theta,\xi,t)$ that of $\dot{u}(\theta,z,t)$. Explicitly,

$$\tilde{\Phi}(r,\theta,\xi,t) = \int_{-\infty}^{+\infty} \Phi(r,\theta,z,t)\exp(-\mathrm{j}\xi z)\,\mathrm{d}z \tag{15}$$

and

$$\tilde{\dot{u}}(\theta,\xi,t) = \int_{-\infty}^{+\infty} \dot{u}(\theta,z,t)\exp(-\mathrm{j}\xi z)\,\mathrm{d}z. \tag{16}$$

These Fourier transforms have to be solutions of the Fourier transform of the governing equations of the fluid behaviour. In cylindrical coordinates, the transform of Helmholtz's equations becomes

$$\frac{\partial^2\tilde{\Phi}(r,\theta,\xi,t)}{\partial r^2} + \frac{1}{r}\frac{\partial\tilde{\Phi}(r,\theta,\xi,t)}{\partial r} + \frac{1}{r^2}\frac{\partial^2\tilde{\Phi}(r,\theta,\xi,t)}{\partial\theta^2} + (k_f^2 - \xi^2)\tilde{\Phi}(r,\theta,\xi,t) = 0. \tag{17}$$

Its solution is found by using separation of variables in the circumferential and radial directions,

$$\tilde{\Phi}(r,\theta,\xi,t) = A(r,\xi)B(\theta,\xi)f(t). \tag{18}$$

The boundary condition (13) on the vibrating elastic shell leads to $f(t) = g(t)$ with $g(t) = \exp(-\mathrm{j}\omega t)$ being the time function of the displacement field. The function $B(\theta,\xi)$ guarantees that the potential function is periodic and continuous,

$$B(\theta,\xi) = \sum_{\gamma=0}^{1}\sum_{k=0}^{\infty} B_k^{\gamma}(\xi)\sin\left(k\theta + \gamma\frac{\pi}{2}\right). \tag{19}$$

In this case, with $B_k^{\gamma}(\xi)$ being real functions and with $B_k(\theta,\xi) = B_k^{\gamma}(\xi)\sin(k\theta + \gamma(\pi/2))$, $\tilde{\Phi}(r,\theta,\xi,t)$ is explicitly defined by

$$\tilde{\Phi}(r,\theta,\xi,t) = \sum_{\gamma=0}^{1}\sum_{k=0}^{\infty} A(r,\xi)B_k(\theta,\xi)f(t). \tag{20}$$

In order to simplify the calculations, we consider a given pair (k, γ). Hence, substituting $\tilde{\Phi}(r, \theta, \xi, t)$ into the Fourier transform of Helmholtz's equation leads to a Bessel differential equation

$$r^2 A_{,rr} + rA_{,r} + (Q_\xi^2 r^2 - k^2)A = 0, \tag{21}$$

where $Q_\xi^2 = k_f^2 - \xi^2$ is the radial wavenumber. The circumferential wavenumber k represents the angular contribution. $A_{,r}$ is the first derivative of A, and $A_{,rr}$ is the second derivative with respect to the radial component r. The use of Sommerfeld's condition and boundary conditions on both the elastic structure and rigid baffles allows us to establish the expression of the Fourier transform of the fluid velocity potential as a function of the Fourier transform of the structural radial velocity. The time derivative of $\tilde{u}(\theta, \xi, t)$ being expanded in the modal basis of the dry shell (9), $\tilde{\Phi}(r, \theta, \xi, t)$ can now be expressed as

$$\tilde{\Phi}(r, \theta, \xi, t) = -\mathrm{j}\omega \sum_{\gamma=0}^{1} \sum_{m=1}^{\infty} \sum_{k=0}^{1} \sum_{l=1}^{3} a_{mki}^{\gamma} \frac{\mathrm{H}_k(Q_\xi r)}{Q_\xi \mathrm{H}_k'(Q_\xi R)} \sin\left(k\theta + \gamma\frac{\pi}{2}\right) \tilde{\Psi}_m(\xi) g(t), \tag{22}$$

where $\tilde{\Psi}_m(\xi)$ is the Fourier transform of a longitudinal mode shape, namely

$$\tilde{\Psi}_m(\xi) = \int_0^L \sin(k_m z) \exp(-\mathrm{j}\xi z)\, \mathrm{d}z. \tag{23}$$

In expression (22), γ denotes the symmetry of modes: $\gamma \in \{0, 1\}$, k is the circumferential wavenumber ($k \equiv n$), and i is the type of mode, $i \in \{1, 2, 3\}$. Moreover, H_k is the kth order Hankel function of the first kind and H_k' is its first derivative with respect to the argument. If Q_ξ is imaginary, Hankel's function of imaginary argument is conveniently replaced by a modified Bessel function of real argument:

$$\mathrm{K}_k(Q_\xi r) = \frac{\pi}{2} \mathrm{j}^{k+1} \mathrm{H}_k(\mathrm{j}Q_\xi r). \tag{24}$$

It is of interest to note that if the fluid medium is assumed to be incompressible, the previous relationship leads to the expression of the Fourier transform of the velocity potential as a function of the modified Bessel function $\mathrm{K}_k(Q_\xi r)$ and its first derivative.

As for the motion of the shell, the motion of the fluid is assumed to be linear. Thus, the pressure variation is related to the velocity potential by the linearized Lagrange relationship,

$$p(r, \theta, z, t) = -\rho_f \frac{\partial \Phi(r, \theta, z, t)}{\partial t}. \tag{25}$$

Once $\tilde{\Phi}(r, \theta, \xi, t)$ is determined, the velocity potential is obtained by using the inverse Fourier transform. Finally, the hydrodynamic pressure fluctuation is defined as a function of the radial acceleration of the wall of the vibrating elastic shell,

$$p(r, \theta, \xi, t) = -\rho_f \omega^2 \sum_{\gamma=0}^{1} \sum_{m=1}^{\infty} \sum_{k=0}^{1} \sum_{l=1}^{3} a_{mki}^{\gamma} \sin\left(k\theta + \gamma\frac{\pi}{2}\right) \int_{-\infty}^{+\infty} \frac{\mathrm{H}_k(Q_\xi r)}{Q_\xi \mathrm{H}_k'(Q_\xi R)} \tilde{\Psi}_m(\xi) \exp(\mathrm{j}\xi z)\, \mathrm{d}\xi\, g(t). \tag{26}$$

2.3. Equation of Motion of the Immersed Cylindrical Shell

The equations of motion for an immersed shell are obtained following the same procedure as for the equations of the dry shell. The matrix equation of motion for an immersed thin

walled shell is

$$[K]\begin{Bmatrix} u \\ v \\ w \end{Bmatrix} + \rho_s h \begin{Bmatrix} \ddot{u} \\ \ddot{v} \\ \ddot{w} \end{Bmatrix} = \begin{Bmatrix} -p|_{r=R} \\ 0 \\ 0 \end{Bmatrix} + \begin{Bmatrix} f_u \\ f_v \\ f_w \end{Bmatrix}. \tag{27}$$

The radial term $p|_{r=R}$ is the hydrodynamic pressure which acts on the shell as a result of the excitation of the external fluid medium, via the vibration of the shell excited by the driving force (1). Relation (27) cannot be used in this form, its left part being expressed in terms of the components of the displacements, while the pressure on the shell walls is defined in terms of the modal magnitudes a^{γ}_{mki}. So, in order to solve the cylinder–fluid coupling problem, we expand the wet shell displacements in the modal basis of the dry structure. Thus, both sides of equation (27) will be expressed using modal amplitudes. With this idea, relation (9) is introduced into equation (27). Using the orthogonality properties of the dry modes, we obtain two independent sets of modal equations of motion. The most difficult part of the calculations is related to the notation, especially keeping track of the subscripts. As in the study of the dry cylinder, three mode shapes are associated with each pair of harmonics (m, n), and the shapes are symmetric or antisymmetric. Therefore, the solution of the coupled problem with the use of the modal basis requires the introduction of four new indices (τ, l, q, j) associated with the coupled modes: τ characterizes the symmetry of the modes $(\tau \equiv \delta)$, l denotes the longitudinal order $(l \equiv m)$, q the circumferential one $(q \equiv n)$ and j the type of deformation mode.

We express the norm of shell mode eigenvectors as

$$N_{lqj} = \frac{\pi R L}{\varepsilon_q}\left[1 + \left(\frac{V_{0lqj}}{U_{0lqj}}\right)^2 + \left(\frac{W_{0lqj}}{U_{0lqj}}\right)^2\right], \tag{28}$$

where ε_q is Neumann's factor: $\varepsilon_q = 1$ if $q = 0$, and $\varepsilon_q = 2$ if $q \neq 0$.

Finally, if we normalize the equation of motion with respect to the mass, we obtain a scalar equation

$$(\omega^2_{lqj} - \omega^2) a^{\tau}_{lqj} = F^{\tau}_{lqj} + P^{\tau}_{alqj}. \tag{29}$$

This expression is established for a given mode (τ, l, q, j); ω_{lqj} is the natural circular frequency of the elastic shell. The second term P^{τ}_{alqj} on the right-hand side characterizes the fluid medium influence on the dynamic behaviour of the elastic shell,

$$P^{\tau}_{alqj} = \omega^2 \frac{\rho_f R}{\rho_s h N_{lqj} \varepsilon_q} \sum_{m=1}^{\infty} \sum_{i=1}^{3} \int_{-\infty}^{+\infty} \frac{\mathrm{H}_k(Q_\xi R)}{Q_\xi \mathrm{H}'_q(Q_\xi R)} \tilde{\Psi}_m(\xi) \tilde{\Psi}^*_l(\xi) \,\mathrm{d}\xi \, a^{\tau}_{mq}, \tag{30}$$

where $\tilde{\Psi}^*_l(\xi)$ is the Fourier transform of the conjugate value of a longitudinal mode shape,

$$\tilde{\Psi}^*_l(\xi) = \int_{-\infty}^{+\infty} \sin(k_l z) \exp(\mathrm{j}\xi z) \,\mathrm{d}z. \tag{31}$$

Expression (30) shows that, although modes with different circumferential wave-numbers q are uncoupled, all modes with identical circumferential order q are coupled via the fluid. In the same way, the three types of modes associated with a pair (m, q) are coupled.

The calculation of the modal component of the generalized force F^{τ}_{lqj} results from the scalar product of the driving force and the displacement of the driving point (R, θ_f, z_f),

$$F^{\tau}_{lqj} = \frac{1}{\rho_s h N_{lqj}} \left[f_u \sin(k_l z_f) \sin\left(q\theta_f + \tau\frac{\pi}{2}\right) + f_v \frac{V^{\tau}_{0lq}}{U^{\tau}_{0lqj}} \sin(k_l z_f) \cos\left(q\theta_f + \tau\frac{\pi}{2}\right) \right.$$

$$\left. + f_w \frac{W^{\tau}_{0lq}}{U^{\tau}_{0lqj}} \cos(k_l z_f) \sin\left(q\theta_f + \tau\frac{\pi}{2}\right) \right]. \tag{32}$$

As for the displacement field (9), this generalized force can be specially written for $\theta = 0$:

$$F^{\tau}_{l0j} = \frac{1}{\rho_s h N_{l0j}} \left[f_u \sin(k_l z_f)\tau + f_v \frac{V^{\tau}_{0l0j}}{U^{\tau}_{0l0j}} \sin(k_l z_f)(1-\tau) + f_w \frac{W^{\tau}_{0l0j}}{U^{\tau}_{0l0j}} \cos(k_l z_f)\tau \right]. \tag{33}$$

Finally, relationship (29), with the associated expressions (30) and (32) or (33), represents one line of the governing matrix equation:

$$([\operatorname{diag} \omega^2_{lqj}] - \omega^2([I] + [M_a]))\{A\} = \{F_{\text{ext}}\}, \tag{34}$$

where $[I]$ is the identity matrix, $[M_a]$ the generalized added mass matrix, $[\operatorname{diag} \omega^2_{lqj}]$ the diagonal matrix of the dry squared circular frequencies, and $\{F_{\text{ext}}\}$ the generalized force vector. $\{A\}$ is the vector of modal magnitudes whose general term is a^{τ}_{lqj}. The effects of the ambient fluid on the vibrations of the elastic structure is readily accounted for by the introduction of a resistance for the compressible fluid, and of an inertia for both the compressible and incompressible fluids. Thus, $[M_a]$ is expressed as a function of the circular eigenfrequency ω. The fluid acts not only as an added mass (real part of $[M_a]$), but also as a radiated loss (imaginary part of $[M_a]$). For low frequencies, this radiative part may be neglected without reducing the accuracy of the solution for the dynamic response of the shell. The previous matrix equation is nonlinear, but $[M_a]$ is constant if the fluid is assumed to be incompressible ($c \to \infty$). In general, the dimension of this matrix set of equations is $3lq$. However, according to equation (30), there is no coupling among circumferential orders, as well as no symmetries of modes (no sum on both q and τ). Finally, the complete dynamic analysis of the submerged baffled shell leads to solving a pair of uncoupled matrix equations (34), these expressions having $3l$ dependent equations.

2.4. Pressure Radiated in Far Field

The pressure radiated by the cylindrical shell at infinity is given by a relationship coming from relation (26). Following Junger & Feit (1972), we use the method of stationary phase.

In spherical coordinates ($z = \rho\cos\varphi$, $r = \rho\sin\varphi$; see Figure 3) and for $\rho \gg R$, the expression of the spatial component of the far-field pressure is

$$p(\rho, \theta, \varphi) = -\rho_f \omega^2 \frac{\mathrm{j}\exp(\mathrm{j}k_f\rho)}{\pi\rho k_f \sin\varphi} \sum_{\gamma=0}^{l} \sum_{m=1}^{\infty} \sum_{k=0}^{\infty} \sum_{i=1}^{3} a^{\gamma}_{mki} \frac{\tilde{\Psi}'_m(k_f\cos\varphi)}{\mathrm{H}'_k(k_f R\sin\varphi)} \sin\left(k\theta + \gamma\frac{\pi}{2}\right)$$

$$\times \exp\left(-\mathrm{j}k\frac{\pi}{2}\right), \tag{35}$$

where

$$\tilde{\Psi}'_m(k_f \cos\varphi) = \begin{cases} \dfrac{2m\pi \cos\left(\dfrac{k_f L \cos\varphi}{2}\right)}{L\left[\left(\dfrac{m\pi}{L}\right)^2 - k_f^2 \cos^2\varphi\right]} & \text{if } m \text{ is odd} \\ \dfrac{2m\pi \sin\left(\dfrac{k_f L \cos\varphi}{2}\right)}{L\left[\left(\dfrac{m\pi}{L}\right)^2 - k_f^2 \cos^2\varphi\right]} & \text{if } m \text{ is even.} \end{cases} \tag{36}$$

Expression (35) is valid for $\rho \gg R$, $\theta \in [0, 2\pi]$ and $\varphi \in [0, \pi]$. Because of the term $\sin\varphi$ in the denominator of the pressure expression, a limiting condition must be used to compute it for $\varphi = 0$ and $\varphi = \pi$. Using the expansion of Hankel's function, it can be shown that $k = 0$ is the only circumferential order which radiates pressure in the axial direction. In fact, if $k \neq 0$ and $\varphi \to 0$ or π, then $\sin\varphi \to 0$ and finally $\mathrm{H}'_k \to \infty$ and $p \to 0$.

As a result, we propose three directivity diagrams: a three-dimensional directivity pattern drawn in Figure 3, and two two-dimensional representations in Figure 4. The three-dimensional directivity pattern is obtained by drawing the pressure at point M belonging to a sphere whose radius is ρ. The two two-dimensional patterns are deduced from the three-dimensional one, with $\theta \in [0, 2\pi]$ and $\varphi \in [0, 2\pi]$.

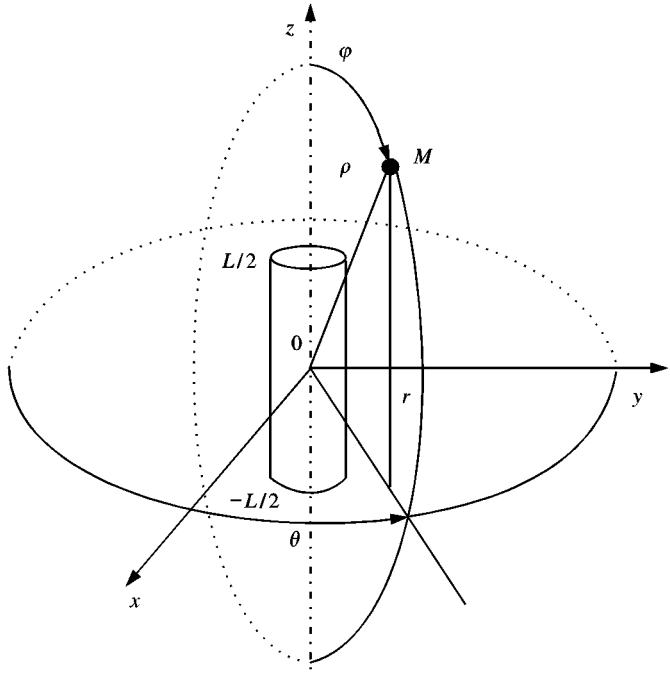

Figure 3. Spherical coordinate system.

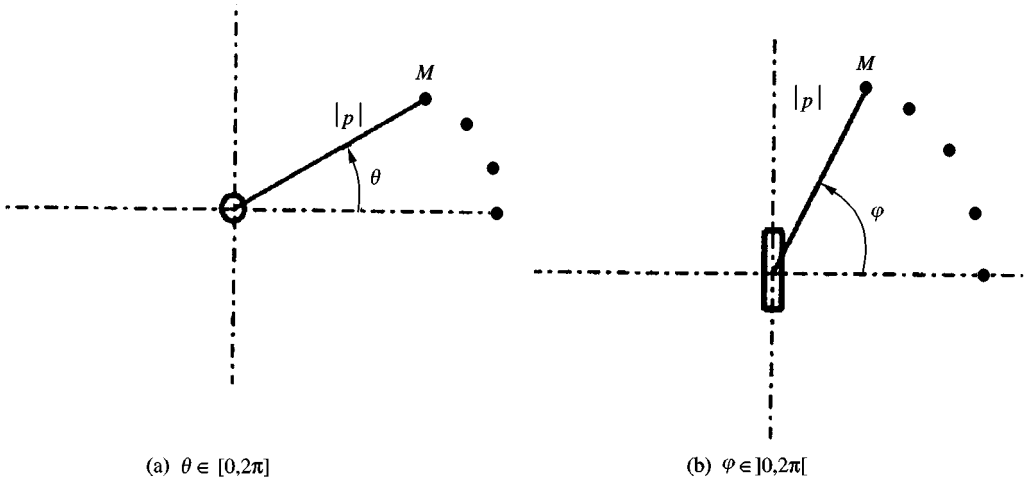

Figure 4. Construction of the two-dimensional directivity patterns. (a) Pressure modulus in the orthogonal plane of the cylinder axis. (b) Pressure modulus in the plane including the cylinder axis.

3. NUMERICAL METHOD FOR THE COUPLED PROBLEM

3.1. Shell Modelling

The shell is discretized into ring finite elements bounded by two parallel planes which are perpendicular to the symmetry axis (Figure 5). The intersections of these planes with the shell middle surface, the nodal circles, have the same purpose as nodal points for two- or three-dimensional finite elements (Grafton & Strome 1963).

Although the geometry of the shell studied is circular (Figure 1), a two-node conical finite element is adopted to discretize the structure (Figure 5). Then, the element can be validated with the previous analytical solution, but also allows us to study any thin cylindrical shell. A ring finite element is completely defined by the nodal radii r_i and r_j, and the longitudinal coordinates z_i and z_j of i and j nodes, respectively.

Using cylindrical coordinates for the analysis of shells of revolution (Figure 6), it is possible to express all quantities such as the boundary conditions, elastic properties, displacements, stresses and strains as periodic functions of the circumferential variable θ. A three-dimensional problem can therefore be reduced to a series of one-dimensional problems. The wall displacements may be expressed in terms of Fourier series,

$$\{U\} = \begin{Bmatrix} u \\ v \\ w \end{Bmatrix} = \begin{Bmatrix} u_0 \\ v_0 \\ w_0 \end{Bmatrix} + \sum_{\delta=0}^{1} \sum_{n=1}^{\infty} \begin{Bmatrix} U_n^{\delta}(s) \sin\left(n\theta + \delta\dfrac{\pi}{2}\right) \\ V_n^{\delta}(s) \cos\left(n\theta + \delta\dfrac{\pi}{2}\right) \\ W_n^{\delta}(s) \sin\left(n\theta + \delta\dfrac{\pi}{2}\right) \end{Bmatrix} g(t), \tag{37}$$

where u is the orthomeridian displacement, v the circumferential displacement and w the meridian displacement. As in the analytical formulation, δ denotes the symmetry of the displacement field (symmetric or antisymmetric) and n denotes the circumferential wavenumber; the case corresponding to the harmonic $n = 0$ is included in the general form (37). In order to take the meridian deformations into consideration, we consider a fourth

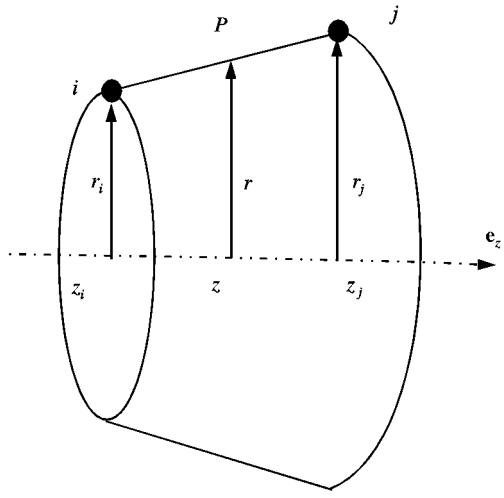

Figure 5. Conical ring finite element idealization.

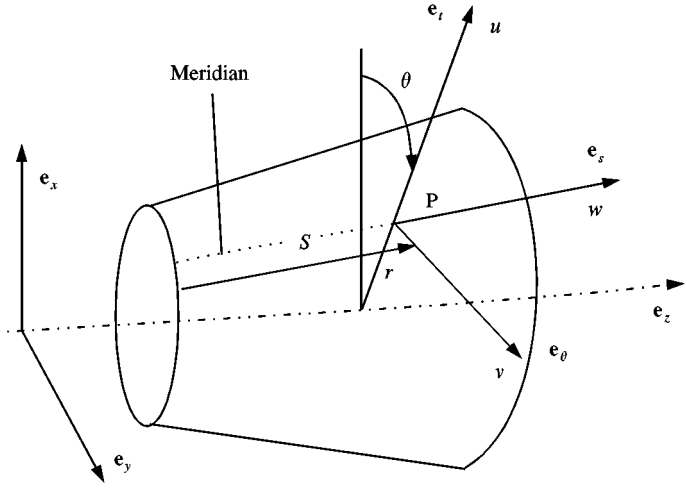

Figure 6. Thin conical shell.

generalized component: the meridian rotation $\beta = u_s$ in the plane including the axis of the shell. With these four components it is possible to describe both the axisymmetric and the non-axisymmetric behaviour of the shell of revolution (Percy *et al.* 1965). $U(s)$, $V(s)$ and $W(s)$ are the longitudinal terms of displacement u, v and w, respectively, at a given meridional position s and time t. These meridian polynomial functions for a conical shell are cubic for the orthomeridian component and linear for the other two:

$$U_n^\delta = \alpha_1 + \alpha_2 s + \alpha_3 s^2 + \alpha_4 s^3,$$
$$V_n^\delta = \alpha_5 + \alpha_6 s, \quad W_n^\delta = \alpha_7 + \alpha_8 s. \tag{38}$$

Moreover, for the case of homogeneous boundary conditions, i.e. when the boundary conditions are independent of the circumferential coordinate θ, there is no coupling between

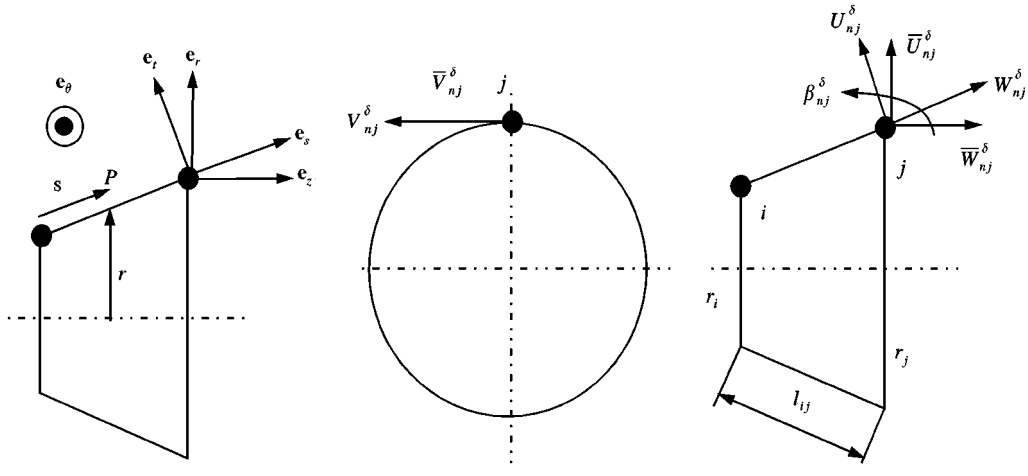

Figure 7. Local and global basis and nodal variables.

the modes of vibration with different circumferential wavenumbers. The vibration problem can then be solved for each pair (n, δ) independently. This is why it is easier to work at a given pair of harmonics (n, δ). Then, we define the components associated with the pair (n, δ) by

$$u_n^\delta = U_n^\delta(s)\sin\left(n\theta + \delta\frac{\pi}{2}\right), \quad v_n^\delta = V_n^\delta(s)\cos\left(n\theta + \delta\frac{\pi}{2}\right),$$
$$w_n^\delta = W_n^\delta(s)\sin\left(n\theta + \delta\frac{\pi}{2}\right), \tag{39}$$

where U_n^δ, V_n^δ, and W_n^δ are the meridian terms of their respective displacements. They can be expressed either in local basis $(\mathbf{e}_t, \mathbf{e}_\theta, \mathbf{e}_s)$ attached to $[i, j]$, or in the global basis $(\mathbf{e}_r, \mathbf{e}_\theta, \mathbf{e}_z)$ attached to the entire structure (Figure 7).

For the chosen two-node finite element, the nodal variables are U_{n*}^δ, V_{n*}^δ, W_{n*}^δ, β_{n*}^δ, where $* = i, j$. These variables are defined in the local basis. In the global basis, the nodal components are $\bar{U}_{n*}^\delta$, $\bar{V}_{n*}^\delta$, $\bar{W}_{n*}^\delta$, $\bar{\beta}_{n*}^\delta$, $* = i, j$. The change of basis is possible using the rotation matrix [Q],

$$\begin{Bmatrix} U_{n^*}^\delta \\ V_{n^*}^\delta \\ W_{n^*}^\delta \\ \beta_{n^*}^\delta \end{Bmatrix} = [Q]\begin{Bmatrix} \bar{U}_{n^*}^\delta \\ \bar{V}_{n^*}^\delta \\ \bar{W}_{n^*}^\delta \\ \bar{\beta}_{n^*}^\delta \end{Bmatrix} \quad \text{with } [Q] = \begin{bmatrix} \cos\varphi & 0 & \sin\varphi & 0 \\ 0 & 1 & 0 & 0 \\ -\sin\varphi & 0 & \cos\varphi & 0 \\ 0 & 0 & 0 & 1 \end{bmatrix}. \tag{40}$$

When the meridian magnitudes of the shell displacements (39) are expressed in terms of the eight nodal variables, we have

$$\{U_n^\delta\} = [\Theta_n^\delta][\mathrm{N}_z]\{a_n^\delta\}_e; \tag{41}$$

$[\mathrm{N}_z]$ is the array of meridian shape functions,

$$[\mathrm{N}_z] = \begin{bmatrix} N_1^u & 0 & 0 & N_2^u & N_3^u & 0 & 0 & N_4^u \\ 0 & N_1^v & 0 & 0 & 0 & N_2^v & 0 & 0 \\ 0 & 0 & N_1^w & 0 & 0 & 0 & N_2^w & 0 \end{bmatrix}. \tag{42}$$

The meridian, tangential and longitudinal shape functions are those defined for the polynomial functions (38), as follows:

$$N_1^u = \frac{1}{4}(1-\xi)^2(2+\xi), \qquad N_2^u = \frac{l_{ij}}{8}(1-\xi^2)(1-\xi),$$

$$N_3^u = \frac{1}{4}(1+\xi)^2(2-\xi), \qquad N_4^u = \frac{l_{ij}}{8}(-1+\xi^2)(1+\xi), \tag{43}$$

$$N_1^v = N_1^w = \frac{1-\xi}{2}, \qquad N_2^v = N_2^w = \frac{1+\xi}{2},$$

with the nondimensional local coordinate $\xi \in [-1, 1]$. $[\Theta_n^\delta]$ is the diagonal array of circumferential terms,

$$[\Theta_n^\delta] = \begin{bmatrix} \sin\left(n\theta + \delta\dfrac{\pi}{2}\right) & 0 & 0 \\ 0 & \cos\left(n\theta + \delta\dfrac{\pi}{2}\right) & 0 \\ 0 & 0 & \sin\left(n\theta + \delta\dfrac{\pi}{2}\right) \end{bmatrix}, \tag{44}$$

where $\{a_n^\delta\}_e$ is the elemental vector of nodal variables associated with a pair (n, δ):

$$\{a_n^\delta\}_e^{\mathrm{T}} = \{U_{ni}^\delta,\ V_{ni}^\delta,\ W_{ni}^\delta,\ \beta_{ni}^\delta,\ U_{nj}^\delta,\ V_{nj}^\delta,\ W_{nj}^\delta,\ \beta_{nj}^\delta\}. \tag{45}$$

In order to determine the mass matrix of a finite element e, we assume a velocity field for e, expressed in terms of generalized nodal velocities. The kinetic energy of the conical element corresponding to the velocity field can thereby given as a function of the nodal variables (45) (Zienckiewicz & Taylor 1991):

$$[M_n]_e = \int_{-1}^{1} \frac{\rho_s \pi h l_{ij}}{\varepsilon_n} [\mathrm{N_s}]^{\mathrm{T}} [\mathrm{N_s}] \left(r_i - \frac{l_{ij}}{2}(1+\xi)\sin\varphi\right) \mathrm{d}\xi. \tag{46}$$

The linear strain–displacement relations (see Appendix B) for a conical shell described in curvilinear coordinates θ and s (Figure 6) have been proposed by Percy *et al.* (1965). When the values of displacements (37) are substituted in these relations, we arrive at equations relating the strains in the shell to the nodal variables $\{a_n^\delta\}_e$. After this, Hooke's law yields the stresses in the conical element:

$$\{\sigma\} = [D]\{\varepsilon\}, \tag{47}$$

where $\{\sigma\}$ is the stress vector, $[D]$ is the elasticity matrix, and $\{\varepsilon\}$ is the strain vector. Accordingly, we obtain the deformation energy and hence the elemental stiffness matrix,

$$[K_n^\delta]_e = \int_{-1}^{1} \frac{\delta \pi h l_{ij}}{\varepsilon_n} [\Pi_n^\delta]^{\mathrm{T}} [D] [\Pi_n^\delta] \left(r_i - \frac{l_{ij}}{2}(1+\xi)\sin\varphi\right) \mathrm{d}\xi, \tag{48}$$

where $[\Pi_n^\delta]$ is defined in Appendix B. As opposed to the mass matrix which depends only on the circumferential order n, this stiffness matrix is a function of both the harmonic order (n) and mode symmetry (δ).

A harmonic point driving force is applied in $[r_f, \theta_f, \xi_f]$ on the mean conical surface. The force is defined as in the analytical formulations (1) and (2), and with $\xi_f \in [-1, 1]$:

$$\{F_n^\delta\}_e = [\mathrm{N}_s(\xi_f)]^\mathrm{T} [\Theta^n(\theta_f)] \begin{Bmatrix} f_u \\ f_v \\ f_w \end{Bmatrix}. \tag{49}$$

It is also possible to define a surface load as an exterior fluid pressure. This pressure p acting on an element involves elemental generalized nodal forces:

$$\{F_{ns}^\delta\}_e = \int_{\partial\Omega_s} [\mathrm{N}_s]^\mathrm{T} [\Theta_n^\delta]^\mathrm{T} \begin{Bmatrix} -p \\ 0 \\ 0 \end{Bmatrix} \mathrm{d}S. \tag{50}$$

Finally, from expressions (46), (48)–(50), we can determine the matrix equation of motion for a thin shell of revolution:

$$[\bar{K}_n^\delta]\{\bar{a}_n^\delta\} + [\bar{M}_n]\{\ddot{\bar{a}}_n^\delta\} = \{\bar{F}_n^\delta\} + \{\bar{F}_{ns}^\delta\}, \tag{51}$$

where $[\bar{K}_n^\delta]$, $[\bar{M}_n^\delta]$, $\{\bar{F}_n^\delta\}$ and $\{\bar{F}_{ns}^\delta\}$ are assembled from elemental matrices. The reference frame changes are operated using the rotation matrix [Q]:

$$[\bar{K}_n^\delta]_e = \begin{bmatrix} [\mathrm{Q}] & [0] \\ [0] & [\mathrm{Q}] \end{bmatrix}^\mathrm{T} [K_n^\delta]_e \begin{bmatrix} [\mathrm{Q}] & [0] \\ [0] & [\mathrm{Q}] \end{bmatrix}. \tag{52}$$

$$[\bar{M}_n^\delta]_e = \begin{bmatrix} [\mathrm{Q}] & [0] \\ [0] & [\mathrm{Q}] \end{bmatrix}^\mathrm{T} [M_n^\delta]_e \begin{bmatrix} [\mathrm{Q}] & [0] \\ [0] & [\mathrm{Q}] \end{bmatrix}. \tag{53}$$

$$[\bar{F}_n^\delta]_e = \begin{bmatrix} [\mathrm{Q}] & [0] \\ [0] & [\mathrm{Q}] \end{bmatrix}^\mathrm{T} [F_n^\delta]_e, \quad \{\bar{F}_{ns}^\delta\}_e = \begin{bmatrix} [\mathrm{Q}] & [0] \\ [0] & [\mathrm{Q}] \end{bmatrix}^\mathrm{T} \{F_{ns}^\delta\}_e. \tag{54, 55}$$

3.2. Fluid Equations

3.2.1. *General boundary element method*

To formulate the coupling between the structure and the external compressible or incompressible fluid, it is necessary to solve the harmonic external Neumann problem for Helmholtz's or Laplace's equation. We assume the ideal compressible medium to have the same characteristics as in the analytical formulation. Hence, the general equations of the external fluid are given by Helmholtz's or Laplace's equation, the boundary condition on the shell, and Sommerfeld's condition at infinity:

(i) Helmholtz or Laplace equation:

$$\Delta\Phi + k_f^2\Phi = 0 \text{ or } \Delta\Phi = 0 \text{ over } \Omega_f; \tag{56}$$

(ii) Sommerfeld's condition at infinity:

$$\lim_{r\to\infty} r\left(\frac{\partial\Phi}{\partial r} - k_f\Phi\right) = 0; \tag{57}$$

(iii) Boundary condition at the shell:

$$\frac{\partial\Phi}{\partial n} = \mathbf{grad}\,\Phi \cdot \mathbf{n} = \mathbf{v}_f \cdot \mathbf{n}. \tag{58}$$

This outer problem is solved using the boundary element method (BEM) (Beer & Watson 1992; Brebia & Dominguez 1992; Hall 1994). The BEM reduces a three-dimensional problem with volume integration to a two-dimensional problem with volume integration to a two-dimensional surface integral. This means that only a description of the fluid–structure interface is necessary, not a complete discretization of the surrounding domain. Thus, the advantage of the BEM formulation is that the solution for unknown parameters will be sought only at the boundary. Using Green's third formula, the fluid problem is transformed into an integral equation

$$\int_{\Omega_f} (\Delta\Phi(P)G(M,P) - \Delta G(M,P)\Phi(P))\,\mathrm{d}\Omega_p = \int_S \left(\frac{\partial G(M,P)}{\partial n_p}\Phi(P) - \frac{\partial \Phi(P)}{\partial n_p}G(M,P)\right)\mathrm{d}S_p, \tag{59}$$

where $\mathbf{n}_p$ is the external surface vector of the shell, Ω_f the fluid domain and $\partial\Omega_f$ the boundary of Ω_f. This surface consists of the surface of the solid S, and that of the boundary at infinity, $\partial\Omega_f = S \cup \partial\Omega_\infty$. If $G(M, P)$ satisfies Sommerfeld's condition), with P belonging to the elastic shell and M located in the three-dimensional domain, is singularity on the interface yields

$$\int_S \left(\Phi(P)\frac{\partial G(M,P)}{\partial n_p} - G(M,P)\frac{\partial \Phi(P)}{\partial n_p}\right)\mathrm{d}S_p = \begin{cases} -4\pi\Phi(M) & \text{if } M \in \Omega_f, \\ -2\pi\Phi(M) & \text{if } M \in S, \\ 0 & \text{if } M \notin \Omega_f \cup S. \end{cases} \tag{60}$$

In a compressible and unbounded fluid, Green's function is defined by

$$G(M,P) = \frac{1}{|MP|}\exp(\mathrm{j}k_f|MP|). \tag{61}$$

k_f being the acoustic wavenumber given in equation (11). When the fluid is assumed to be incompressible, Green's function becomes

$$G(M,P) = \frac{1}{|MP|}. \tag{62}$$

The potential function Φ which satisfies Helmholtz's (or Laplace's) equation (11) is established using the method of singularities. This method is based on the fact that Helmholtz's or Laplace's equation is linear. Then, the velocity potential Φ must be considered as a linear combination of elementary potentials, each of them satisfying Helmholtz's or Laplace's equation as well as Sommerfeld's condition. These elementary potentials can be produced by evenly distributed singularities such as normal dipoles or sources (Susbielle & Bratu 1981; Delhommeau 1987). Considering a mixed Green distribution, located at a point P on the fluid–shell interface S, a density of sources and normal dipoles is defined as

$$\sigma(P) = \frac{\partial \Phi}{\partial n_p} \quad \text{and} \quad \mu(P) = -\Phi(P). \tag{63}$$

According to the definition of the normal derivative of Φ, the distribution of sources can be associated with the normal velocity on the interface S. The distribution of normal dipoles is equal to the velocity potential on the surface S. Then, the only unknown variable of this

fluid problem is the distribution of normal dipoles $\mu(P)$ on the surface. Expression (60) is written for a point M belonging to the structure surface S. With a mixed Green's distribution and discontinuities of potential generated by sources and dipoles across the interface, we can express the following Fredholm relationship of the second kind:

$$\frac{\mu(M)}{2} - \frac{1}{4\pi}\int_S \mu(P)\frac{\partial G(M,P)}{\partial n_P}\,\mathrm{d}S_p = \frac{1}{4\pi}\int_S \sigma(P)G(M,P)\,\mathrm{d}S_p. \tag{64}$$

We use a subdomain collocation method to solve the integral equation. The interface S is discretized by N_f boundary elements. The surface integrals of equation (64) on this surface are transformed into a sum of integrals calculated on each boundary element. With this aim, the Fredholm equation is written for P located at the centroid M_J of panel J and M located at the centroid M_I of panel I:

$$\frac{\mu_I}{2} - \frac{1}{4\pi}\sum_{J=1}^{N_f}\mu_J\int_{S_J}\frac{\partial G_{IJ}}{\partial n_J}\,\mathrm{d}S_J = \frac{1}{4\pi}\sum_{J=1}^{N_f}\sigma_J\int_{S_I} G_{IJ}\,\mathrm{d}S_J. \tag{65}$$

According to equations (61) or (62), the Green's function associated to M_I and M_J is defined by

$$G_{IJ} = G(M_I, M_J) = \frac{\exp(\mathrm{j}k_f|M_IM_J|)}{|M_IM_J|} \quad \text{or} \quad G_{IJ} = \frac{1}{|M_IM_J|}. \tag{66}$$

Furthermore, the normal derivatives of G_{IJ} are

$$\frac{\partial G_{IJ}}{\partial n_J} = \mathbf{grad}_{M_J}(G(M_I, M_J))\cdot\mathbf{n}_J. \tag{67}$$

For each element I, there is a relationship like equation (65). Such a relation expresses the influence of every panel J on panel I. Finally, equation (65) is a typical line of the following global set of equations which must be solved to study the fluid problem:

$$[D]\{\mu\} = [S]\{\sigma\}, \tag{68}$$

where $[D]$ is the array of normal-dipole influence coefficients and $[S]$ is the matrix of source influence coefficients.

3.2.2. *Plane boundary element*

In the general case with an interface S of any shape, this interface is discretized by N_f quadrilateral or triangular plate panels (Figure 8). Every panel is characterized by the coordinates of its geometric centre, the components of its unit normal vector and its area S_I such that $S = \lim_{N_f\to\infty}\sum_{I=1}^{N_f} S_I$; S_I is supposed to be sufficiently small to support a constant density of sources and normal dipoles. On S_I, $\mu(P)$ and $\sigma(P)$ remain equal to their mean values μ_I and σ_I, respectively, calculated at the centroid.

The general element of $[D]$ is

$$D_{IJ} = \frac{1}{2}\delta_{IJ} - \frac{1}{4\pi}\int_{S_J}\frac{\partial G_{IJ}}{\partial n_J}\,\mathrm{d}S_J, \tag{69}$$

δ_{IJ} being the Kronecker delta; $[S]$ is the matrix of source influence coefficients and its general element has the following form:

$$S_{IJ} = \frac{1}{4\pi}\int_{S_J} G_{IJ}\,\mathrm{d}S_J. \tag{70}$$

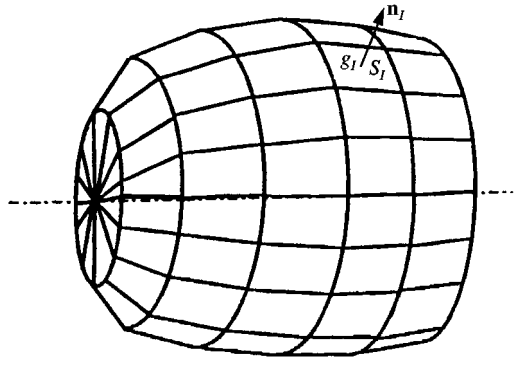

Figure 8. Plane boundary panel mesh.

3.2.3. *Ring boundary element*

In the case of a cylindrical geometry, the interface S is discretized by N_f conical ring boundary elements (Figures 9 and 10).

As in the modelling of the shell, the interface geometry allows us to express the surface quantities into a series of the angular variable θ. Every boundary element I is characterized by its reference meridian line ($\theta = 0$) of length l_I and spatially by the coordinates of its centroid g_I, the components of its unit normal vector $\mathbf{n}_I$ and its surface S_I.

Meridian lines are supposed to be sufficiently short to support a constant density of sources and normal dipoles. On every line, $\mu(P)$ and $\sigma(P)$ remain equal to their mean values, μ_{nl} and σ_{nl}, respectively. These values are calculated at the centroid of the meridian line (Figure 10). Thus, the distributions of singularities can be expanded into Fourier series,

$$\sigma_I = \sum_{n=0}^{\infty} \sigma_{nI} \cos(n\theta_I), \quad \mu_I = \sum_{n=0}^{\infty} \mu_{nI} \cos(n\theta_I). \tag{71, 72}$$

Expression (64) is written for $\theta_I = 0$ and a given circumferential half-wavenumber n. It expresses the influence of every ring boundary element on the reference meridian line of the element I. For each ring boundary element I, there is a relationship like equation (65). This expression describes the influence of every element J on the element I. Finally, equation (65) is a typical line of the following global system which must be solved in order to study the fluid problem:

$$[D_n]\{\mu_n\} = [S_n]\{\sigma_n\}. \tag{73}$$

In this case, the general element of $[D_n]$ is

$$D_{nIJ} = \frac{\delta_{IJ}}{2} - \frac{1}{4\pi} \int_{S_J} \frac{\partial G_{IJ}}{\partial n_J} \cos(n\theta_J)\, \mathrm{d}S_J, \tag{74}$$

δ_{IJ} being the Kronecker delta; and the general element of the matrix of sources influence coefficients $[S_n]$ is

$$S_{nIJ} = \frac{1}{4\pi} \int_{S_J} G_{IJ} \cos(n\theta_J)\, \mathrm{d}S_J. \tag{75}$$

Furthermore, σ_{nJ} and μ_{nJ} are the general elements of the vectors of meridian densities of sources and normal dipoles, respectively. The coefficients in equations (74) and (75) are evaluated by numerical integration.

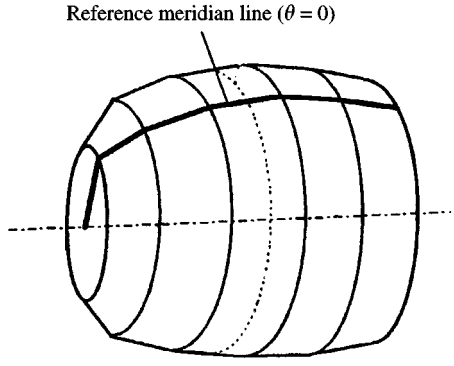

Figure 9. Ring boundary element mesh.

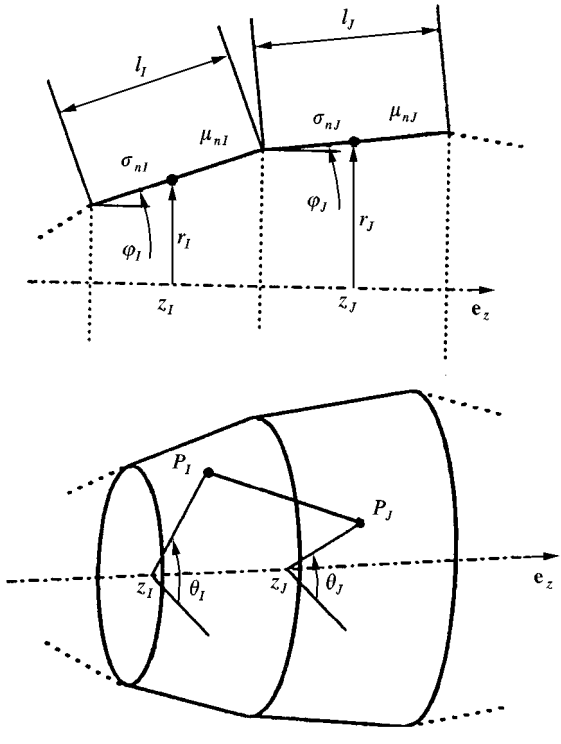

Figure 10. Geometrical characteristics.

3.3. Coupling Fem–Bem

The coupling between the two models is made for each conical ring finite element (discretization of the shell) and each boundary elements facing it (discretization of the fluid). It is therefore necessary to define an elemental coupling matrix $[FS]_e$ which connects the normal velocities $\{V_n^\delta\}_e$ on boundary elements to the elementary shell nodal velocities as follows:

$$\{V_n^\delta\}_e = [FS]_e \{\dot{a}_n^\delta\}_e. \tag{76}$$

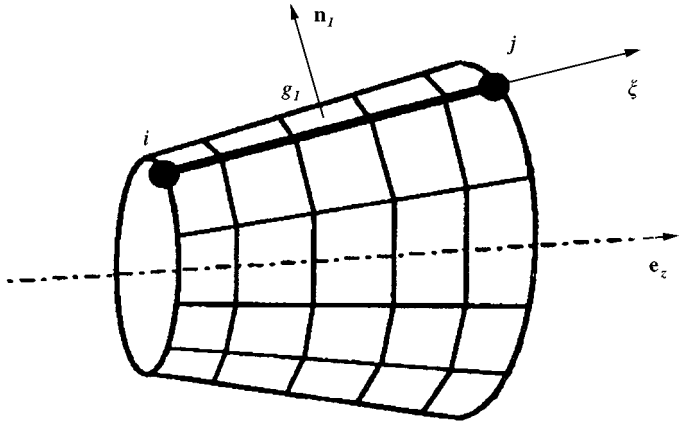

Figure 11. Coupling of ring finite element (shell) and plane boundary panels (interface).

When we consider the plane boundary elements (Figure 11), the structural discretization and knowledge of the local coordinates (θ_I, ξ_I) of the panel centres allow us to define the elemental coupling matrix in terms of the interpolation functions (41) (Delhommeau *et al.* 1981; Oudin *et al.* 1984; Peseux & Quevat 1985):

$$\{V_n^\delta\}_e = \begin{bmatrix} \cdot \\ \cdot \\ \cdot \\ \{n_I\}^t[\Theta_n^\delta(\theta_I)](\mathrm{N}_s(\xi_I)] \\ \cdot \\ \cdot \\ \cdot \end{bmatrix} \{\dot{a}_n^\delta\}_e = [FS_n^\delta]_e \{\dot{a}_n^\delta\}_e, \tag{77}$$

where $[\mathrm{N}_s(\xi_I)]$ and $[\Theta_n^\delta(\theta_I)]$ are, respectively, the matrix of meridian interpolation functions and the matrix of angular terms of the finite element expressed at the geometric centre of the current panel; $\{n_I\}$ represents the components of the normal unit vector of the current panel. The matrix $[FS_n^\delta]_e$ depends on both the circumferential order n and symmetry δ and can be written as

$$[FS_n^\delta]_e = \begin{bmatrix} \vdots & & & & & & & \vdots \\ N_1^u(\xi_I) & 0 & 0 & N_2^u(\xi_I) & N_3^u(\xi_I) & N_3^u(\xi_I) & 0 & 0 & N_4^u(\xi_I) \\ \vdots & & & & & & & \vdots \end{bmatrix} \sin\left(n\theta_I + \delta\frac{\pi}{2}\right). \tag{78}$$

The number of lines in $[FS_n^\delta]_e$ is equal to the number of panels associated with the finite element e. The number of rows is equal to the number of degrees of freedom of e, i.e., eight.

When we consider the ring boundary elements (Figure 12), the elemental coupling matrix in equation (77) is independent of the circumferential number n:

$$[FS]_e = \begin{bmatrix} \vdots & & & & & & & \vdots \\ N_1^u(\xi_I) & 0 & 0 & N_2^u(\xi_I) & N_3^u(\xi_I) & 0 & 0 & N_4^u(\xi_I) \\ \vdots & & & & & & & \vdots \end{bmatrix}. \tag{79}$$

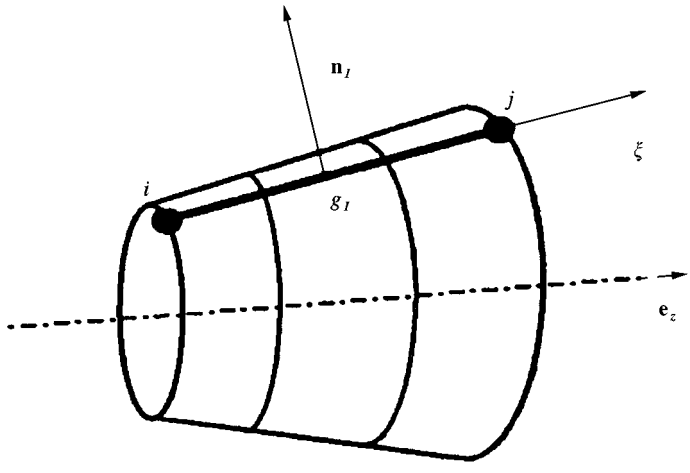

Figure 12. Coupling of ring finite element (shell) and ring boundary elements (interface).

The corresponding elemental coupling matrices, in the global basis are

$$[\overline{FS}_n^\delta]_e = [FS_n^\delta]_e \begin{bmatrix} [Q] & [0] \\ [0] & [Q] \end{bmatrix} \quad \text{or} \quad [\overline{FS}]_e = [FS]_e \begin{bmatrix} [Q] & [0] \\ [0] & [Q] \end{bmatrix}. \tag{80}$$

Finally, the coupling between the complete discretization of the shell of revolution and all the boundary elements requires to assemble all the elemental coupling matrices. The entire coupling can be written as follows:

$$\{\bar{V}_n^\delta\} = [FS_n^\delta]\{\dot{\bar{a}}_n^\delta\} \quad \text{or} \quad \{\bar{V}_n^\delta\} = [\overline{FS}]\{\dot{\bar{a}}_n^\delta\}. \tag{81}$$

3.4. Governing Equations of the Submerged Shell

The previous fluid analysis using the boundary element method has allowed us to express the density vector of normal dipoles as a function of the distribution of sources on boundary elements. The distribution of sources can be likened to the normal velocities of the shell and the distribution of normal dipoles to the velocity potential on each boundary element. Thus, expression (68) leads us to express the velocity potential at the centre of each boundary element in terms of the normal velocity at these points:

$$\{\Phi_n^\delta\} = -[D]^{-1}[S]\{V_n^\delta\} \qquad \text{or} \qquad \{\Phi_n^\delta\} = -[D_n]^{-1}[S_n]\{V_n^\delta\}. \tag{82}$$

Then, the pressure fluctuation in the fluid medium can be evaluated from the velocity potential using Lagrange's linearized formula (25). Thus, equations (76) and (82) give the following relationship between the surface pressure and the shell nodal vector of velocities:

$$\{p_n^\delta\} = \rho_f \frac{\partial}{\partial t}([D]^{-1}[S][\overline{FS}_n^\delta]\{\dot{\bar{a}}_n^\delta\}) \qquad \text{or} \qquad \{p_n^\delta\} = \rho_f \frac{\partial}{\partial t}([D]^{-1}[S][FS]\{\dot{\bar{a}}_n^\delta\}). \tag{83}$$

The general element of $\{p_n^\delta\}$ is the pressure p_{In}^δ on a boundary element I.

Finally, it is possible to write the vector of nodal generalized forces equivalent to the surface pressures. According to equation (50), and taking plane boundary elements, we have

$$\{F_{ns}^{\delta}\}_e = \sum_{I=1}^{N_k} \int_{S_J} [\mathrm{N}_s(\xi_I)]^{\mathrm{T}} [\Phi_n^{\delta}(\theta)]^{\mathrm{T}} \begin{Bmatrix} -p_{In}^{\delta} \\ 0 \\ 0 \end{Bmatrix} \mathrm{d}S_J. \tag{84}$$

where N_{fe} is the number of boundary elements facing the finite element e. This expression may be given in a matrix form

$$\{\bar{F}_{ns}^{\delta}\} = -\rho_f [\overline{FS}_n^{\delta}]^{\mathrm{T}} [A_f] [D]^{-1} [S] [\overline{FS}_n^{\delta}] \{\ddot{\bar{a}}_n^{\delta}\}. \tag{85}$$

where $[A_f]$ is the diagonal array of panel surfaces; its dimension is N_f and has the following form:

$$[A_f] = \begin{bmatrix} \ddots & 0 & 0 \\ 0 & S_J & 0 \\ 0 & 0 & \ddots \end{bmatrix}. \tag{86}$$

In the same way, with ring boundary elements, equations (84)–(86) become

$$\{F_{ns}^{\delta}\}_e = \sum_{I=1}^{N_{ft}} \int_{S_j} [\mathrm{N}_s(\xi_I)]^{\mathrm{T}} [\Theta_n^{\delta}(\theta)]^{\mathrm{T}} \begin{Bmatrix} -p_{In}^{\delta} \sin\left(n\theta + \delta\dfrac{\pi}{2}\right) \\ 0 \\ 0 \end{Bmatrix} \mathrm{d}S_J. \tag{87}$$

$$\{\bar{F}_{ns}^{\delta}\} = -\frac{\rho_f}{\varepsilon_n} [\overline{FS}]^{\mathrm{T}} [A_f] [D]^{-1} [S] [\overline{FS}] \{\ddot{\bar{a}}_n^{\delta}\}. \tag{88}$$

$$[A_f] = 2\pi \begin{bmatrix} \ddots & 0 & 0 \\ 0 & r_J l_J & 0 \\ 0 & 0 & \ddots \end{bmatrix}. \tag{89}$$

Using expression (51) of the governing matrix equation of a shell of revolution loaded by both point and surface loads, the matrix equation of motion for a submerged axisymmetric shell becomes

$$[\bar{K}_n^{\delta}] \{\bar{a}_n^{\delta}\} + ([\bar{M}_n] + [\bar{M}_{an}^{\delta}]) \{\ddot{\bar{a}}_n^{\delta}\} = \{\bar{F}_n^{\delta}\}. \tag{90}$$

The generalized added mass $[\bar{M}_{an}^{\delta}]$ is obtained from Equations (85) or (88) and is expressed in the global basis. As equation (90) is written for a given circumferential wavenumber n, it must be solved for each n in order to completely study the vibro-acoustic behaviour of the shell (but only the first few lowest values of n are of importance from an engineering point of view).

3.5. External Pressure Field

The displacements of the immersed thin cylindrical shell are given by the equation of motion, equation (90). The nodal variables can be used to calculate the velocity potential and the surface pressure on each boundary element using (63) and (68).

Afterwards, the radiated pressure is obtained using the potential expression (60) and Lagrange's linearized equation. Like the displacements of the shell, the pressure at point

M in the compressible medium is determined for each pair of harmonic (n, δ) from the third Green's formula

$$p_n^\delta(M) = -\frac{j\omega}{4\pi}\int_S \left(\Phi_n^\delta(P)\frac{\partial G(M,P)}{\partial n_P} - G(M,P)\frac{\partial \Phi_n^\delta(P)}{\partial n_P}\right) dS_p. \tag{91}$$

Using the plane–panel discretization, this expression becomes

$$p_n^\delta(M) = -\frac{j\omega}{4\pi}\sum_{l=1}^{N_f}\int_{S_l}\left(\Phi_{nI}^\delta\frac{\partial G(M,M_I)}{\partial n_I} - G(M,M_I)\frac{\partial \Phi_{nI}^\delta}{\partial n_I}\right) dS_I. \tag{92}$$

and using the ring boundary element discretization, we get

$$p_n^\delta(M) = -\frac{j\omega}{4\pi}\sum_{l=1}^{N_f}\int_{S_l}\left(\Phi_{nI}^\delta\frac{\partial G(M,M_I)}{\partial n_I} - G(M,M_I)\frac{\partial \Phi_{nI}^\delta}{\partial n_I}\right)\sin\left(n\theta_I + \delta\frac{\pi}{2}\right) dS_I. \tag{93}$$

For each harmonic, the pressure p_n^δ is proportional to the amplitude of the corresponding displacement of the shell and, finally, the pressure variation generated by the elastic vibrating shell of revolution is obtained by summation of these harmonic contributions:

$$p(M) = \sum_{\delta=0}^{1}\sum_{n=0}^{\infty} p_n^\delta(M). \tag{94}$$

3.6. Comparison of the Fluid–Structure Models

In a coupled problem, it is first necessary to define exactly both the amplitude and the shape of the shell. Secondly, it is necessary to make the behavior of the solid shell pass onto the fluid-structure interface. There are therefore two strategies to solve such a problem (Bérot 1997).

The first approach involves considering the fluid-structure boundary as a rigid surface. Then, the influence coefficients of singularity are determined at the interface without any hypothesis on its motion. Only the mutual position of each boundary element is taken into account. Matrices $[D]$ and $[S]$ are invariant and are calculated before the structural finite element analysis. Afterwards, it is necessary to define exactly the amplitude and the shape of the shell facing the interface. Each point of this fluid-structure boundary is given the acceleration of the solid point facing it through a coupling matrix. This matrix $[\overline{FS}_n^\delta]$, binding the solid shell and the fluid-structure interface, is defined as a function of circumferential harmonics. Such an approach is used in the numerical model which couples ring finite elements and plane boundary elements.

The second strategy consists in giving only the amplitude of the shell to the fluid-structure interface. With this point of view, it is not possible to consider the fluid-structure boundary as a rigid body. It is necessary to define an interface shape similar to the shell shape and to establish the associated singularity distributions. This procedure is used in the model which couples ring finite elements with ring boundary elements.

The shape of the fluid-structure interface sometimes allows us to reduce the amount of data exchanged between the structural analysis and the fluid problem. Hence, only the amplitude of the structural shape is imparted to the boundary element discretization by the finite element modeling. The fact that there is little information to transfer between the two domains in the solution process leads to significantly reduced dimensions of the matrices

associated with the coupled problem. The second boundary element discretization implies that $[D_n] \equiv [D]$ and $[S_n] \equiv [S]$ are calculated for each circumferential order. This approach is only possible for cases in which the shapes of fluid-structure interface are simple and is therefore very useful for bodies of revolution.

4. NUMERICAL RESULTS

4.1. Cylindrical Shell

In what follows, all the results presented are obtained for a steel cylinder immersed in an heavy fluid (water) (Bérot & Peseux 1996, 1997). The mechanical characteristics of the shell are: Young's modulus $E = 2 \times 10^{11}$ N/m^2, Poisson's ratio $\nu = 0{\cdot}3$, density $\rho_s = 7850$ kg/m^3; the geometrical characteristics are: length $L = 1{\cdot}2$ m; mean radius $R = 0{\cdot}4$ m; thickness $h = 0{\cdot}003$ m. The water density is $\rho_f = 1000$ kg/m^3 and the sound velocity $c = 1500$ m/s. In order to determine the directivity diagrams, the thin cylinder is excited by a harmonic driving force located at point $z = L/2$ and $\theta = 0$. According to relation (1), the components of the unit driving force are $F = (1, 0, 0)$ N. The pressure is calculated at point M belonging to a sphere whose radius $\rho = 150$ m (Figure 3).

4.1.1. *Analytical formulation*

In the analytical formulation of an immersed baffled cylinder in the first part of the paper (Section 2), there are two steps of calculation. The first one requires the determination of the modal characteristics, i.e. eigenfrequencies and eigenvectors, of the dry elastic structure. Figure 1 presents the geometry of the analytical model. The wall velocity is equal to zero on both infinite baffles, but the elastic thin shell imports a velocity field at the fluid–structure interface.

Figure 13 presents general variations of the three frequencies obtained with Flügge's theory, for each pair of harmonics (m, n). We can see that the eigenfrequencies associated with deflection [Figure 13(a)] are smaller than the others associated with torsion [Figure 13(b)] and extension [Figure 13(c)]. The numerical values corresponding to Flügge's and Donnell's theories are given in Table 1.

The second step in the study of the dynamic behaviour of an immersed circular thin shell concerns the definition of the modal basis. From a theoretical point of view, the matrices in equation (34) have infinite dimensions. To make this formulation practical, it is necessary to truncate the longitudinal modal basis. To validate this truncation, one must evaluate the severity of its effects on the response of the immersed shell. In a light fluid ($\rho_f \ll \rho_s$), cross-modal coupling can be neglected with small effect on the dynamic behaviour of the shell, but if the cylinder is submerged in a heavy fluid ($\rho_f/\rho_s \approx 1$), the coupling of longitudinal half-wavenumbers cannot be neglected.

Figure 14(a–c) shows the effect of truncation of the longitudinal basis on the modal amplitude associated with a few circumferential orders q. These calculations are for a cylindrical shell immersed in water, excited by a time-harmonic point driving force applied to the mid-shell surface at $z = L/2$. This figure shows that a wide expansion of the longitudinal basis is necessary to have good results, especially for low circumferential wavenumber. The asymptotic character of modal amplitudes is confirmed by a numerical results. For each point of the curve, the dimension of the longitudinal basis is $l_{\max}$, i.e. $l \in [1, l_{\max}]$. For three circumferential wavenumbers ($q = 1$, $q = 2$ and $q = 5$) and for five frequencies tested ($f = 50$, 100, 150, 200 and 300 Hz), Figure 14(a–c) shows that the order of the longitudinal basis has the same effect; i.e. the convergence is slow as $l_{\max}$ increases.

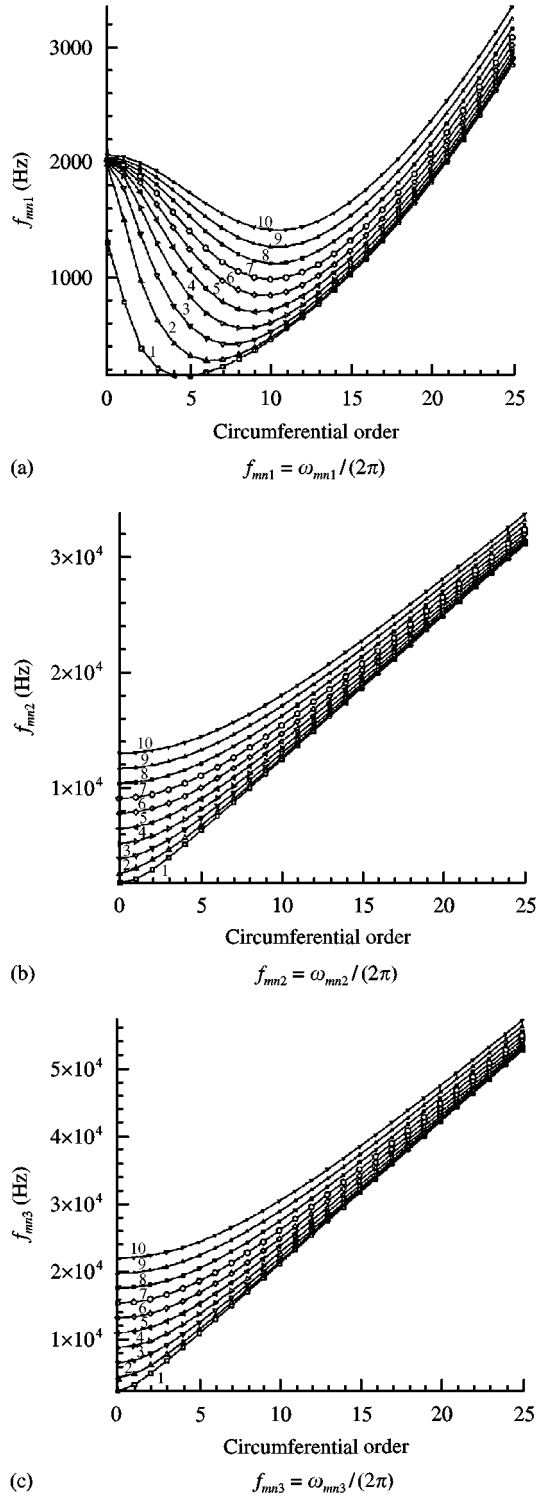

Figure 13. Eigenfrequencies of a simply supported dry cylinder, $n \in [0, 25]$, $m \in [1, 10]$, according to Flügge's theory; from Leissa (1973).

TABLE 1

Eigenfrequencies of a simply supported dry cylindrical shell; frequencies in Hz

Theory										
$i = 1$										
m, n	1, 5	1, 4	1, 6	1, 3	1, 7	2, 6	2, 7	1, 8	2, 5	2, 8
Donnell	142·9	145·7	176·7	210·4	230·1	281·1	290·8	296·3	321·3	334·5
Flügge	139·1	143·4	172·4	209·5	225·6	278·1	286·9	291·7	319·3	330·1
$i = 2$										
m, n	1, 0	1, 1	2, 0	1, 2	2, 1	2, 2	3, 0	1, 3	3, 1	2, 3
Donnell	1304·0	2147·0	2609·0	2962·0	3092·0	3815·0	3913·0	4024·0	4182·0	4698·0
Flügge	1304·0	2147·0	2609·0	2962·0	3092·0	3815·0	3913·0	4024·0	4182·0	4698·0
$i = 3$										
m, n	1, 0	1, 1	2, 0	2, 1	1, 2	2, 2	3, 0	1, 3	3, 1	2, 3
Donnell	2461·0	3428·0	4466·0	4986·0	5100·0	6255·0	6647·0	6972·0	6987·0	7879·0
Flügge	2461·0	3428·0	4466·0	4986·0	5100·0	6255·0	6647·0	6972·0	6987·0	7879·0

TABLE 2

Eigenfrequencies of a simply supported cylindrical shell immersed in water; frequencies in Hz

Theory										
$i = 1$										
m, n	1, 4	1, 5	1, 3	1, 6	1, 7	2, 6	1, 2	2, 7	2, 5	1, 8
Donnell	66·4	69·9	88·5	91·8	125·8	148·8	149·7	161·1	161·6	169·1
Flügge	65·4	68·1	88·1	89·6	123·4	147·2	149·7	158·9	160·6	166·5
$i = 2$										
m, n	1, 0	1, 1	2, 0	1, 2	2, 1	2, 2	3, 0	1, 3	3, 1	2, 3
Donnell	1304·0	1843·0	2608·0	2834·0	2914·0	3640·0	3913·0	3970·0	4118·0	4698·0
Flügge	1304·0	1843·0	2608·0	2834·0	2914·0	3640·0	3913·0	3970·0	4118·0	4698·0
$i = 3$										
m, n	1, 0	1, 1	2, 0	2, 1	1, 2	2, 2	3, 0	1, 3	3, 1	2, 3
Donnell	2212·0	3076·0	4415·0	4898·0	4794·0	6120·0	6619·0	6735·0	6949·0	7879·0
Flügge	2212·0	3076·0	4415·0	4898·0	4794·0	6120·0	6619·0	6735·0	6949·0	7879·0

For the five frequencies tested and in terms of the circumferential order, we calculate the response corresponding to a minimal basis $l_{max} = 1$ and to a larger basis $l_{max} = 21$. Figure 15 shows the relative differences between the two results. This figure shows that the internodal coupling has not been neglected in the calculation of modal amplitudes of a baffled cylinder immersed in a heavy fluid. Nevertheless, the number of terms in the longitudinal modal basis has little effect on the frequency response of the submerged shell. The fluid may be either light or heavy, but a smaller expansion basis will give good results.

The same study and the same comparisons are made for an immersed cylinder. Figure 16(a–c) shows the three resonant frequencies associated with a pair (m, n) for a shell immersed in a heavy fluid. The numerical values calculated with our coupled formulation based on the analytical shell theories from Flügge and Donnell, are presented in Table 2. We can see that the ambient medium has a weak influence on the frequencies associated with both torsion ($i = 2$) and extension-compression ($i = 3$) movements. It does not

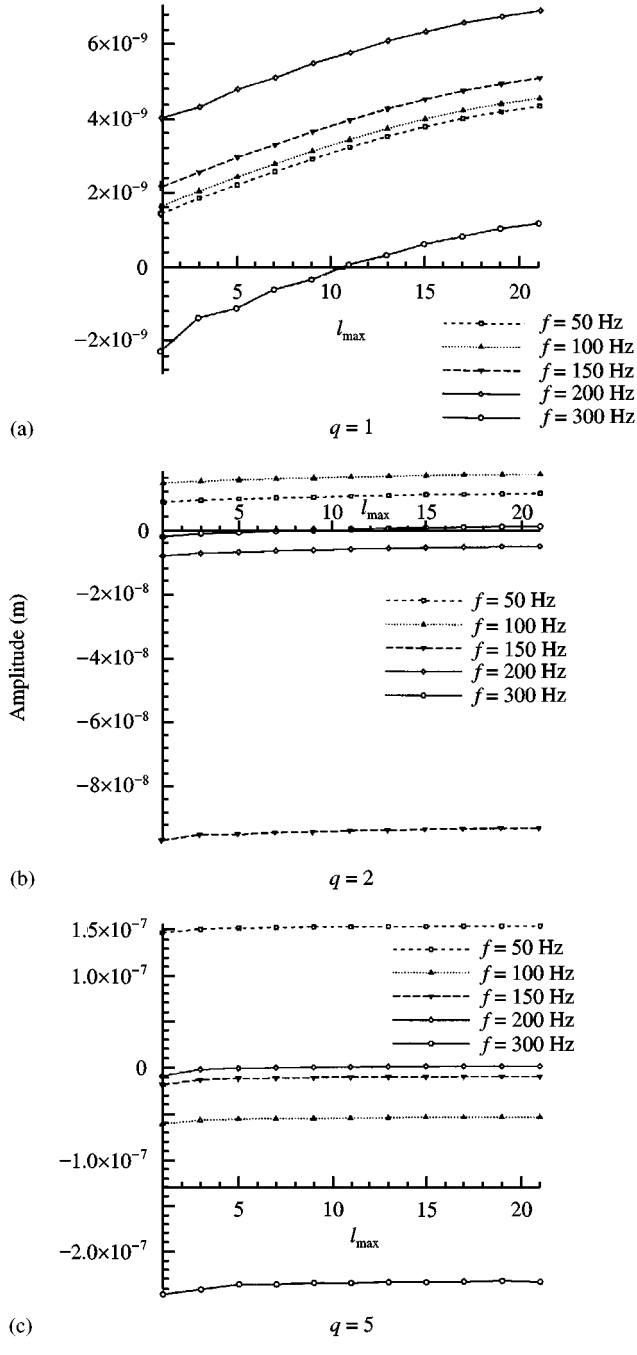

Figure 14. Influence of the number of terms in the longitudinal modal basis on modal amplitudes.

influence the pure torsional modes ($i = 2$ and $n = 0$); in an inviscid fluid, the outer fluid medium has no influence on these components of the displacement field. Tables c1 and c2, in Appendix C, give all the analytical values associated to Flügge's theory, concerning both the dry and immersed cylinder. Thus, calculating the resonant frequencies is numerically easy, even if the calculation of the radiated pressure involves an important amount of CPU time.

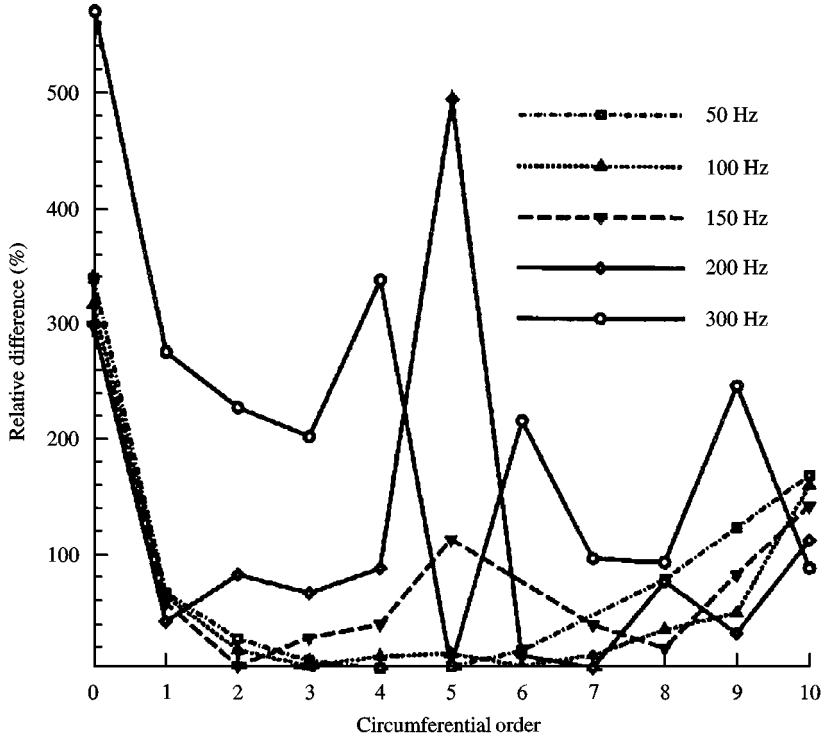

Figure 15. Relative differences on modal amplitude between a minimal and a larger basis.

The modal method decomposes the vibrations in a series of circumferential modes. It is therefore necessary to choose the modes which significantly contribute to the amplitude of the wall. Figure 17 presents the contribution of the first ten circumferential orders in five driving frequencies.

If the curves in Figure 17 are compared to Figure 14(a–c), it appears that there is no final conclusion about the choice of the circumferential basis expansion, and for any excitation frequency it is very difficult to predict the contribution of each circumferential wavenumber on the final response. Of course, if the excitation frequency coincides with the frequency associated with the resonant mode, this mode has a large influence.

Like the displacements of the immersed shell, the pressure radiated in the far field is a function of the longitudinal modal basis. It is not necessary to develop this basis to a large extent in order to have accurate results (Laulagnet & Guyader 1989, 1990). As opposed to the calculation of the amplitude of the wall displacements at a given frequency, the directivity patterns (constructed according to Figures 3 and 4) associated with an uncoupled circumferential wavenumber q. We use only the circumferential orders which have a resonant frequency below the excitation frequency. In fact, it appears that the modes related to low circumferential wavenumbers have a large influence on the pressure radiated in the far field.

4.1.2. *Numerical model*

The coupled numerical model is validated using the previous analytical formulation. Two comparisons are proposed. The first one concerns the resonant frequencies of the submerged shell and the second is about the pressure radiated in the far field. The thin elastic shell is modelled using 22 ring finite elements, amounting to 23 nodes (Figure 18).

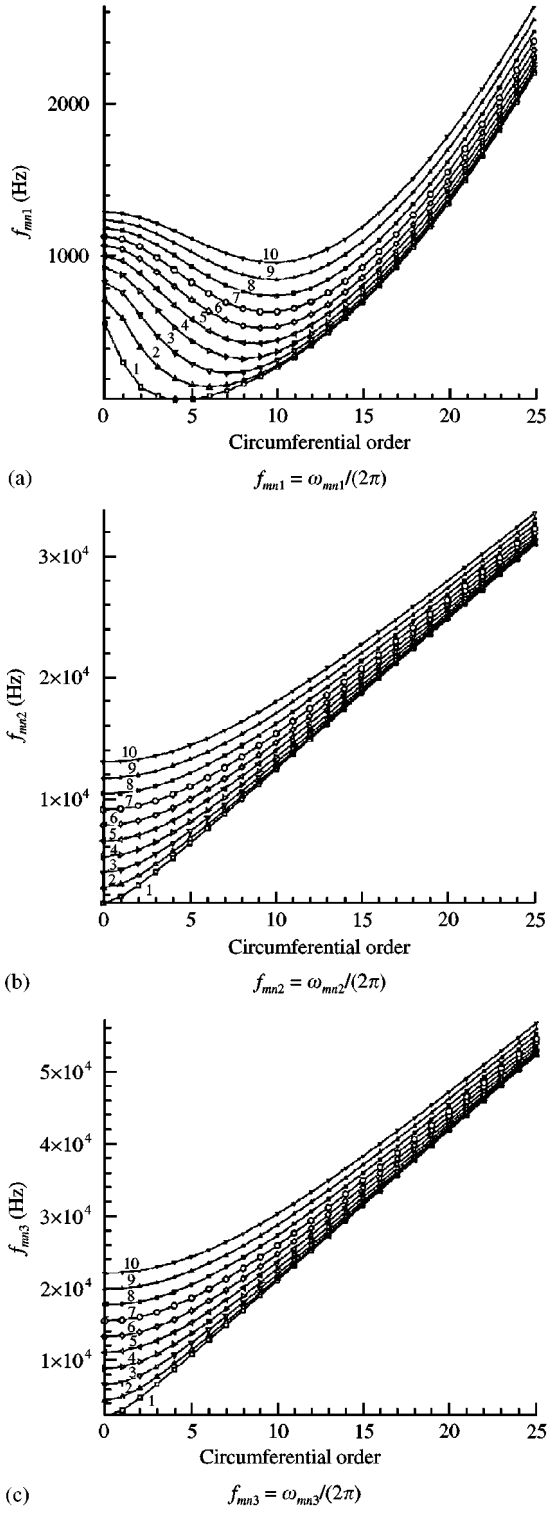

Figure 16. Eigenfrequencies of a simply supported immersed cylinder, $n \in [0, 25]$, $m \in [1, 10]$, according to Flügge's theory; from Leissa (1973).

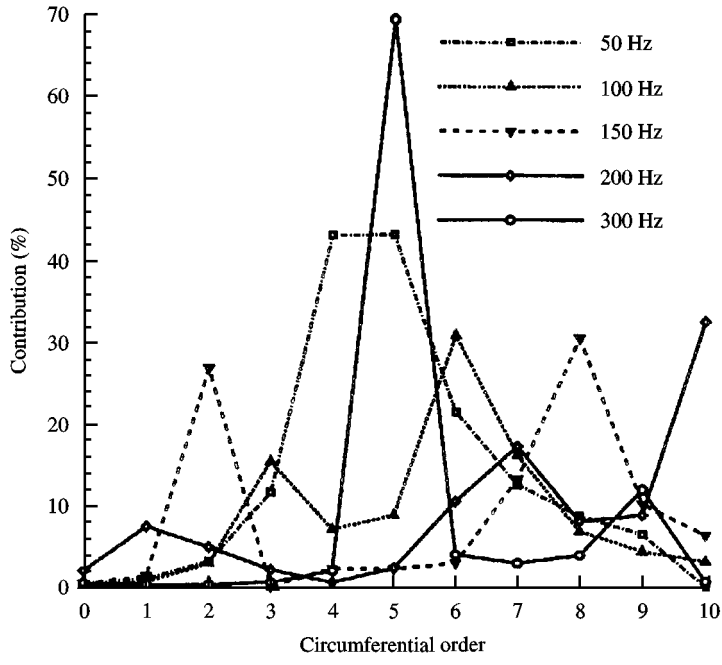

Figure 17. Contribution to the amplitude displacement of the circumferential modes.

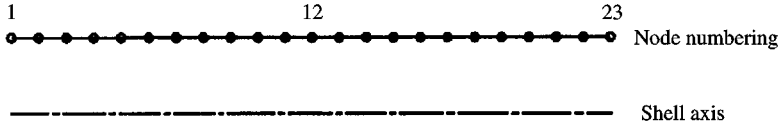

Figure 18. Structural model.

According to the boundary conditions given in Section 2.1, the nodal variables at the extremities of the vibrating cylinder are $U_n^\delta = V_n^\delta = 0$. Figures 19 and 20 show the two modelling representations of the immersed baffled cylinder.

It appears that the infinite rigid baffles have no influence on either the resonant frequencies or the pressure radiated in the far field. The dynamic behaviour of a finite cylinder is the same as that of a baffled cylindrical shell. The modelling of the fluid–structure interface with plane panels requires different numbers of boundary elements depending on the parameter being predicted. The calculation of the resonant frequencies requires only three to four plane panels per circumferential wavenumber, while the determination of the radiated pressure requires eight plane panels per circumferential wavenumber. Below eight boundary elements, the velocity distribution on the vibrating wall is usually not modelled properly.

Table 3 gives the frequencies of the dry cylinder calculated with the conical ring finite element. The values are compared to the previous analytical frequencies corresponding to the first shape mode $i = 1$. The different results are in good agreement.

In Table 4, we compare the numerical eigenfrequencies obtained with the two coupled models: ring finite elements coupled with plane panels, and ring finite elements coupled with ring boundary elements *vis-à-vis* the analytical results corresponding to Flügge's theory. The fluid–structure interface, when we use the planar panel, is idealized with one plane

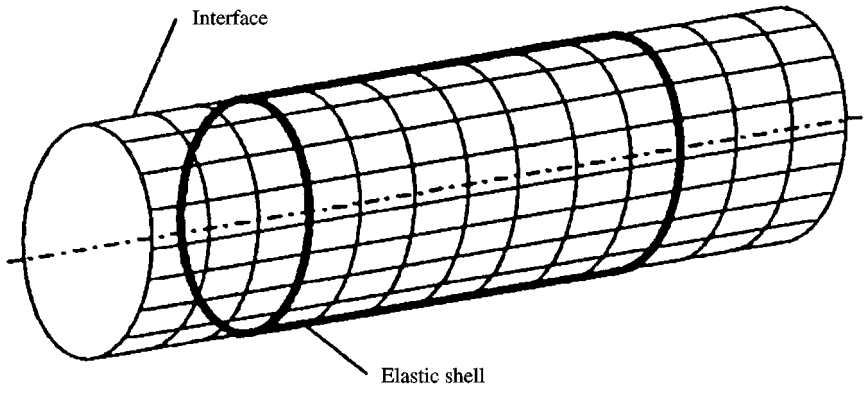

Figure 19. Numerical coupled model: planar panel/ring finite element coupling.

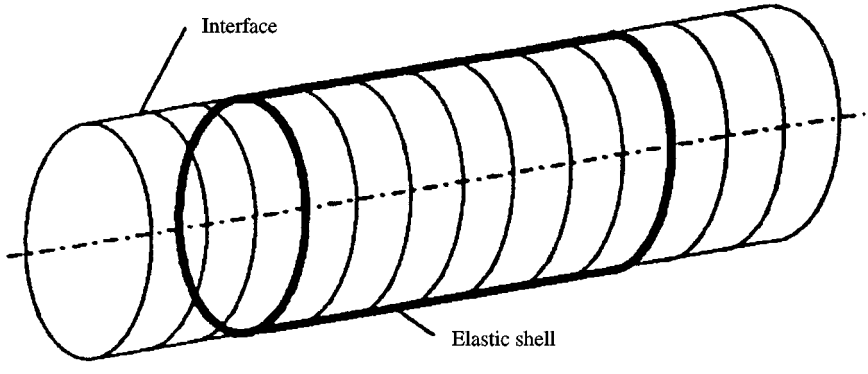

Figure 20. Numerical coupled model: ring boundary element/ring finite element coupling.

TABLE 3

Dry cylindrical shell; frequencies in Hz

Theory $i = 1$ m, n	1, 5	1, 4	1, 6	1, 3	1, 7	2, 6	2, 7	1, 8	2, 5	2, 8
Donnell	142·9	145·7	176·7	210·4	230·1	281·1	290·8	296·3	321·3	334·5
Flügge	139·1	143·4	172·4	209·5	225·6	278·1	286·9	291·7	319·3	330·1
Numerical n	5	4	6	3	7	6	7	8	5	8
Ring*	139·7	144·1	172·6	210·4	226·0	280·9	288·4	291·8	322·9	331·5

*22 conical ring finite elements.

TABLE 4

Cylindrical shell immersed in water; frequencies in Hz

Theory $i = 1$ m, n	1, 4	1, 5	1, 3	1, 6	1, 7	2, 6	1, 2	2, 7	2, 5	1, 8
Flügge	65·4	68·1	88·1	89·6	123·4	147·2	149·7	158·9	160·6	166·5
Numerical n	4	5	3	6	7	2	6	7	5	8
Ring*	65·6	68·4	87·9	90·0	123·8	146·8	148·9	160·4	162·6	167·0
Ring†	66·2	69·1	88·6	90·9	125·4	147·6	150·5	162·2	163·8	169·4

*22 conical ring finite elements coupled with 550 plane panels.
†22 conical ring finite elements coupled with 22 ring boundary elements.

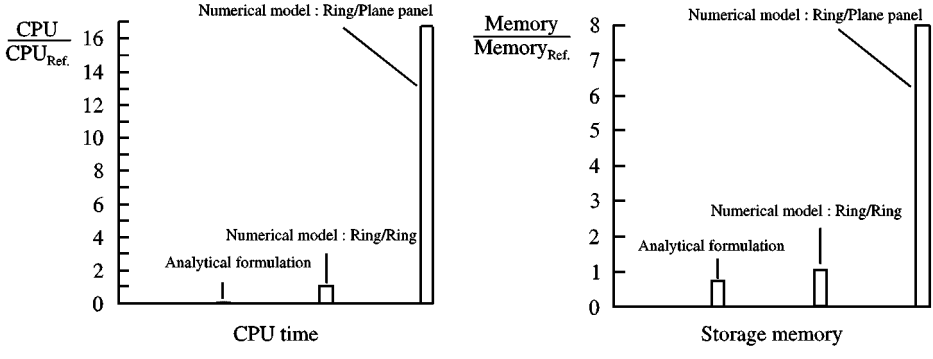

Figure 21. CPU time and storage memory to calculate the first twenty resonant frequencies. ($CPU_{Ref.}$ = CPU time corresponding to the ring/ring model, $Memory_{Ref.}$ = Memory storage corresponding to the ring/ring model).

panel for each finite element meridian and 25 boundary elements on the circumference. With the second numerical model, the fluid–structure interface is idealized with one ring boundary element for each ring finite element. Here also we can notice a very good agreement between the different values.

Figure 21 presents a comparison of the CPU time and storage memory required to calculate the first 20 resonant frequencies by both the analytical formulation and the numerical models. As a reference, we take into account the CPU time and the storage memory corresponding to the use of the numerical model which couples ring finite elements and ring boundary elements.

Figures 22–24 present the directivity diagrams associated with different circumferential orders. The directivity patterns are constructed according to Figures 3 and 4, and with a coordinate system centred at $z = L/2$. As was previously written, $n = 0$ is the only mode which radiates pressure in the axial direction. Circumferential modes $n = 3$ and $n = 5$, as well as any other nonzero n, do not produce any pressure in the direction.

Figures 25–27 show the directivity patterns calculated at a given driving frequency by summation of the elementary diagrams related to each circumferential order. The pressure is calculated for each circumferential order independently. Afterwards, the pressure radiated

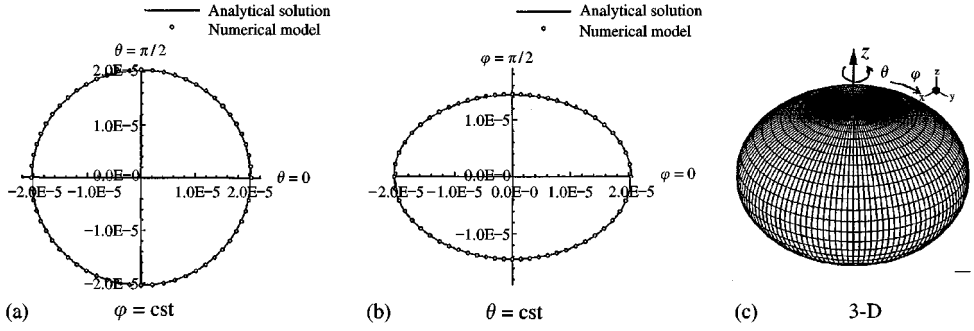

Figure 22. Directivity diagrams associated with $n = 0$ for $f = 60$ Hz.

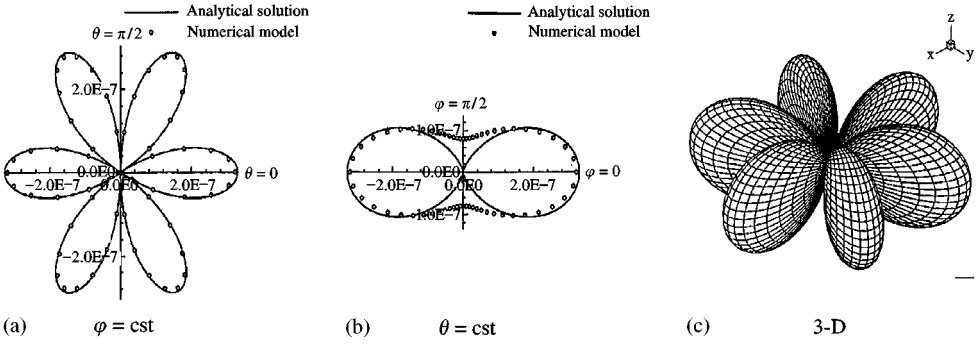

Figure 23. Directivity diagrams associated with $n = 3$ for $f = 60$ Hz.

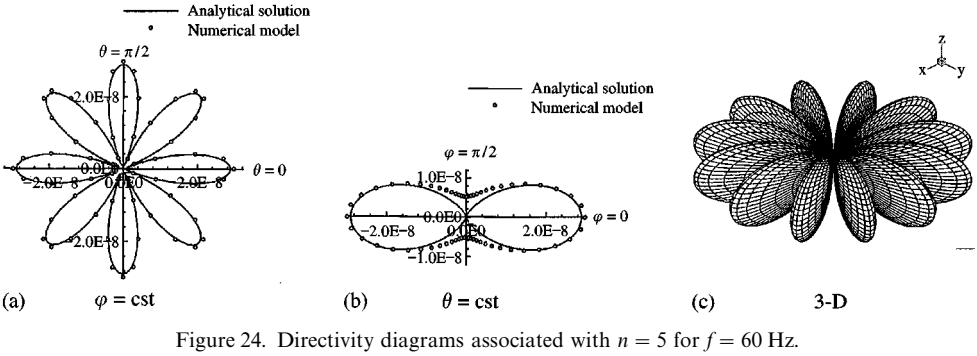

Figure 24. Directivity diagrams associated with $n = 5$ for $f = 60$ Hz.

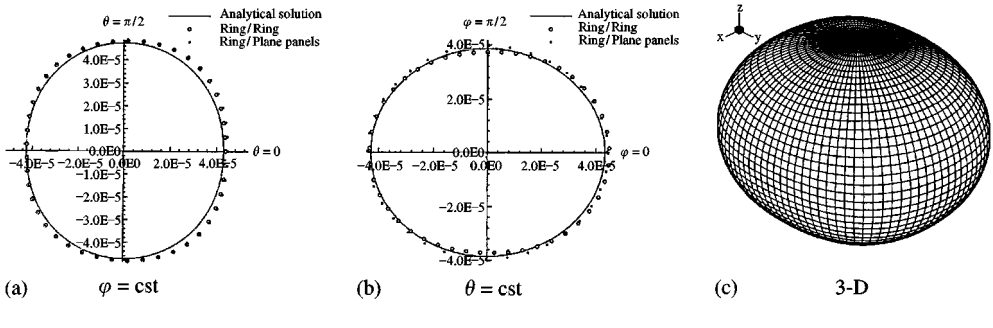

Figure 25. Directivity patterns for $f = 80$ Hz; $n \in [0, 5]$.

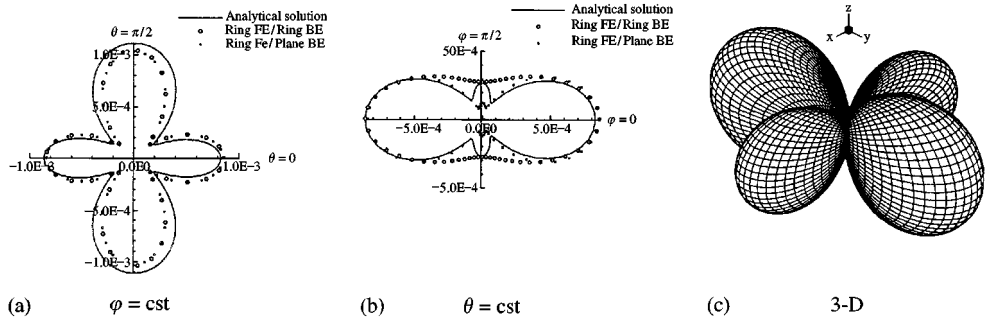

Figure 26. Directivity patterns for $f = 140$ Hz; $n \in [0, 7]$.

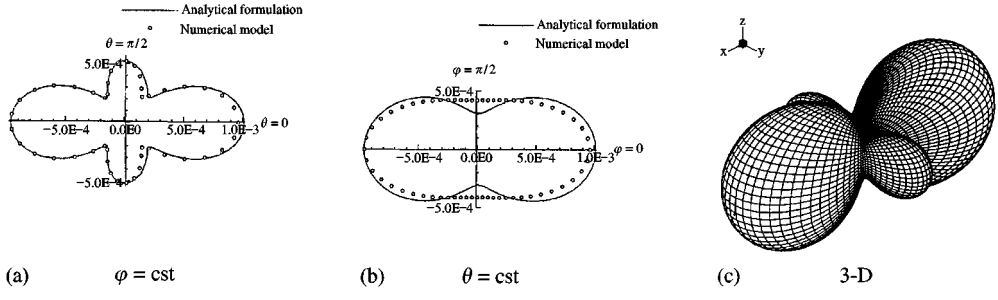

Figure 27. Directivity patterns for $f = 160$ Hz; $n \in [0, 8]$.

at a given frequency is obtained by summation of these elementary pressure fields [equations (93) and (94)]. The driving frequency considered is $f = 80$ Hz in Figure 25, $f = 140$ Hz in Figure 26, $f = 160$ Hz in Figure 27, and the circumferential wavenumbers are respectively $n \in [0, 5]$, $n \in [0, 7]$ and $n \in [0, 5]$.

Figure 28 presents a comparison between CPU time and storage memory required to obtain the directivity diagram corresponding to Figure 25(b) ($f = 80$ Hz, $\theta = \text{cst}$) calculated by both the analytical formulation and the numerical models. As previously, the reference is the numerical model which couples ring finite elements with ring boundary elements.

For directivity patterns in the radial direction [part (a) of each figure], the numerical models and the numerical solution coincide. There are however a few differences in the axial direction (b). Actually, these differences can be justified by the inaccurate representation of the "infinite" rigid baffles.

The calculation of the resonant frequencies with the numerical model coupling ring finite elements to ring boundary elements and the determination of directivity patterns required less storage memory and CPU time than the numerical model which couples ring finite elements to plane boundary elements. In the two significant tests, the calculation using the ring/ring model involved the same cost as the analytical solution, but allows us to model shells of revolution which are not necessarily circular.

4.2. Spherical Shell

The numerical model developed here can be used for the study of any shell of revolution. Hence, the second application presented here concerns a thin spherical shell (Hayeck 1966), and the model used is the ring-finite-element/ring-boundary-element coupling. The shell of revolution is idealized into an assembly of 40 ring finite elements. The hydroelastic and

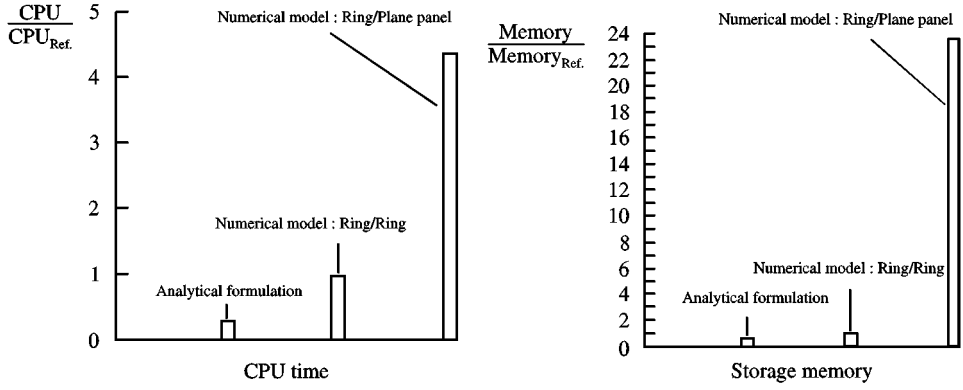

Figure 28. CPU time and storage memory to obtain a 2-D directivity diagram like the one found in Figure 25(b) ($f = 80$ Hz, θ = cst).

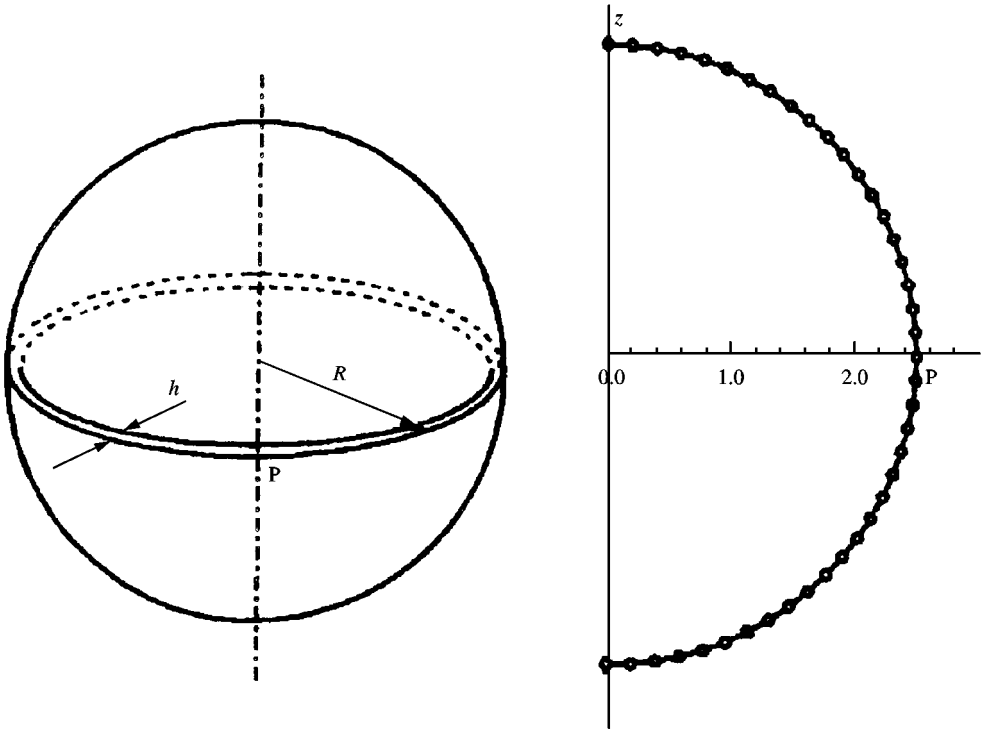

Figure 29. Idealization of a thin spherical shell.

vibroacoustic studies can also use 40 ring boundary elements. The shell is studied without prescribed displacement.

The mechanical characteristics of the shell are: Young's modulus $E = 2{\cdot}1 \times 10^{11}$ N/m^2, Poisson's ratio $\nu = 0{\cdot}3$, density $\rho_s = 7850$ kg/m^3; its geometrical characteristics are: mean radius $R = 2{\cdot}5$ m, thickness $h = 0{\cdot}01$ m (Figure 29).

Figure 30 presents the first 20 resonant frequencies associated with the first 11 circumferential orders of the dry sphere, except for two eigenfrequencies related to the rigid modes ($f = 0$ Hz). In the same way, Figure 31 shows the resonant frequencies of the structure immersed in water.

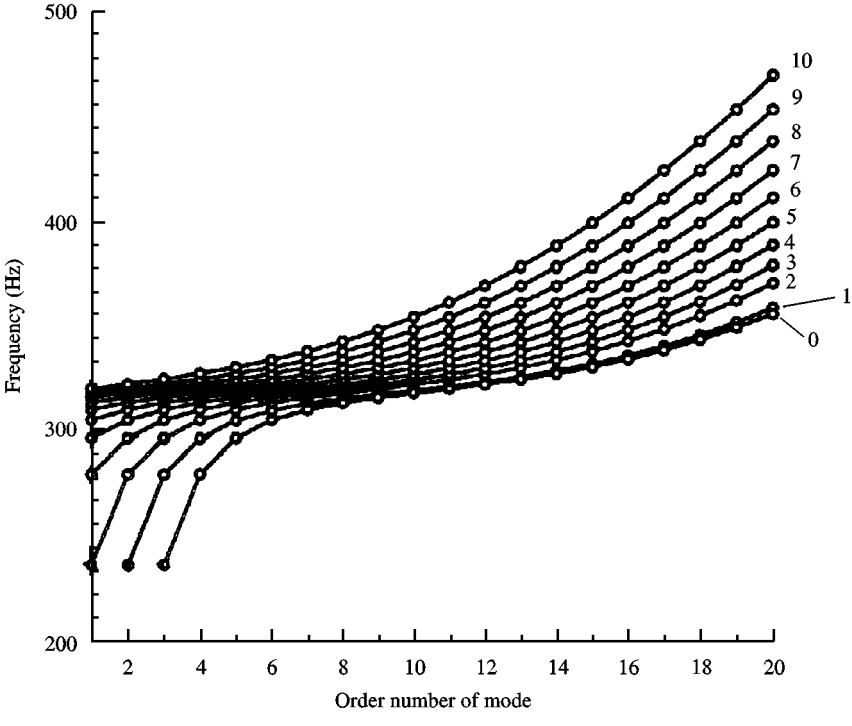

Figure 30. Eigenfrequencies of a dry spherical shell.

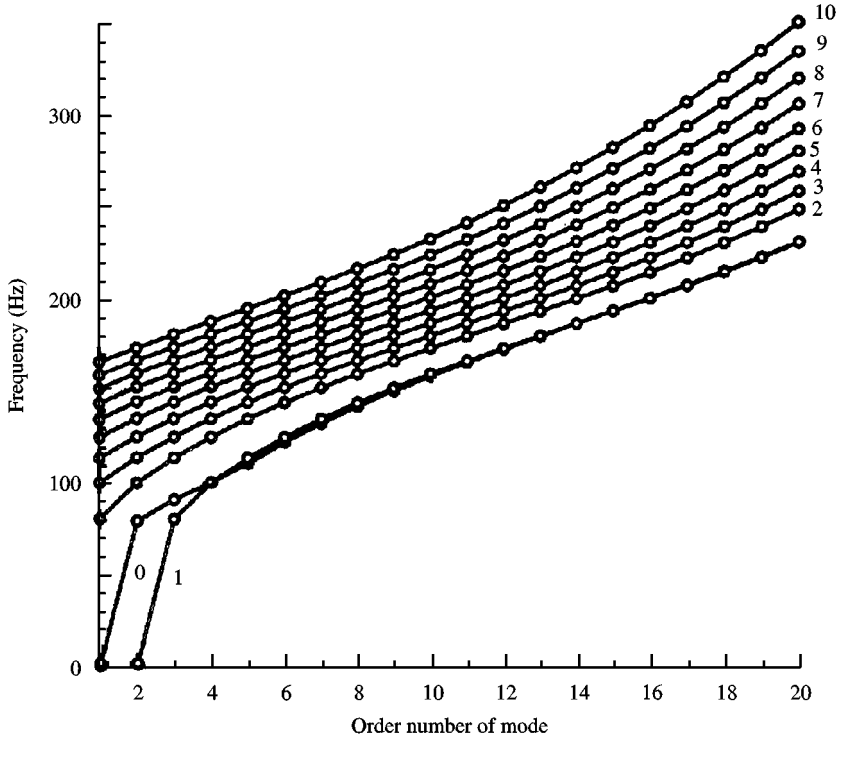

Figure 31. Eigenfrequencies of an immersed spherical shell.

TABLE 5

Dry spherical shell; frequencies in Hz. Theory: from Peseux (1989)

		f_1	f_2	f_3	f_4	f_5	f_6	f_7	f_8
Theory		236·12	279·6	296·7	305·2	310·1	313·4	315·8	317·8
$n = 0$	Ring*	236·1	279·6	296·7	305·2	310·1	313·4	315·8	317·9
	Ring†	236·8	280·0	297·0	305·6	310·9	314·6	316·0	319·0
$n = 1$	Ring*	236·1	279·6	296·7	305·2	310·2	313·4	315·9	318·0
	Ring†	236·5	280·4	297·8	306·2	311·4	314·7	317·3	320·3
$n = 2$	Ring*	237·3	280·7	297·7	306·1	310·9	314·1	316·6	318·7
	Ring†	236·6	280·3	297·8	306·4	311·6	315·0	318·7	319·0
$n = 3$	Ring*	–	279·6	296·8	305·3	310·3	313·6	316·1	318·2
	Ring†	–	280·3	298·0	306·5	311·8	315·4	319·3	319·5
$n = 4$	Ring*	–	–	296·7	305·2	310·1	313·4	315·8	317·9
	Ring†	–	–	297·6	306·7	312·3	315·9	318·7	322·3
$n = 5$	Ring*	–	–	–	305·2	310·1	313·3	315·8	323·3
	Ring†	–	–	–	306·6	312·1	316·1	320·2	320·5

*20 ring curved finite elements; from Peseux (1989).
†40 ring finite elements (present study).

TABLE 6

Sphere immersed in water; frequencies in Hz. Theory: from Peseux (1989)

		f_0 (Inflating)	f_1	f_2	f_3	f_4	f_5	f_6	f_7
Theory		94·8	80·7	100·1	113·7	124·6	133·8	141·9	149·2
$n = 0$	Ring*	94·3	80·6	99·4	112·1	122·1	129·7	136·4	141·0
	Ring†	91·3	79·6	100·7	111·1	122·9	132·8	142·2	150·5
$n = 1$	Ring*	–	80·4	99·1	112·0	121·4	129·2	135·9	141·5
	Ring†	–	81·1	100·7	114·6	126·0	136·0	145·0	153·2
$n = 2$	Ring*	–	81·2	101·0	113·0	122·0	130·0	137·1	142·2
	Ring†	–	81·2	100·9	115·0	126·3	136·2	145·1	153·2
$n = 3$	Ring†	–	–	101·0	115·2	126·6	136·4	145·3	153·5
$n = 4$	Ring†	–	–	–	115·1	126·8	136·7	145·7	153·7
$n = 5$	Ring†	–	–	–	–	126·8	137·0	146·0	154·0

*18 curved ring finite elements coupled with 360 plane panels; from Peseux (1989).
†40 ring finite coupled with 40 ring boundary elements (present study).

The numerical eigenfrequencies of the present model are presented in Table 5 for the dry spherical shell and in Table 6 for the immersed spherical shell and are compared to those obtained by Peseux (1989). These results concern an analytical formulation based on the work from Naghdi & Kalnins (1962) and numerical results obtained with the use of curved ring finite element developed by Wielgosz (1976).

Figures 30 and 31 show that the eigenfrequencies of a spherical shell have a high multiplicity order (coinciding frequencies). For example, there are three resonant frequencies of the submerged shell around 100 Hz. In the same way, there are four eigenfrequencies for the dry shell around 279 Hz. This phenomenon is true for each frequency for both a dry

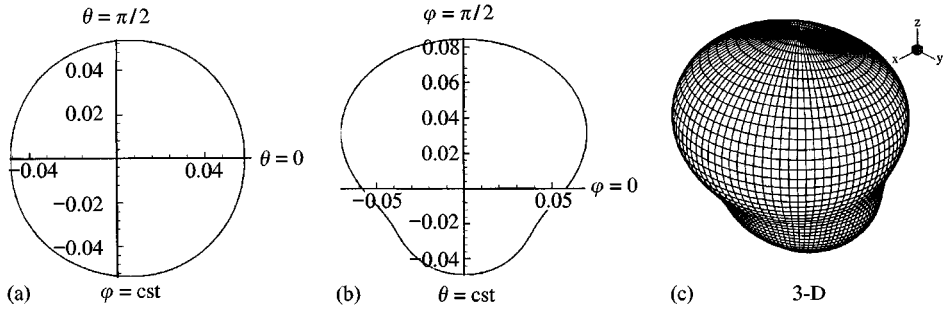

Figure 32. Directivity patterns for driving frequency $f = 114{\cdot}5$ Hz; $n = [0, 5]$.

and a submerged sphere, except for the inflating mode ($n = 0$) of the dry sphere ($f = 543$ Hz, not computed here) and of the immersed shell ($f \approx 94$ Hz).

Figure 32 shows the directivity pattern drawn at a distance $\rho = 150$ m from the centre of the sphere. It is obtained in the case of a point force applied at $\theta = 0$ and $\varphi = \pi/2$, and for the excitation frequency $f = 114{\cdot}5$ Hz, the wavenumbers taken into account are $n \in [0, 5]$.

5. CONCLUSION

In this paper, we have presented two different approaches for the study of the dynamical behaviour of a thin shell of revolution immersed in an incompressible (hydroelastic dynamics) or in a compressible fluid (vibro-acoustic dynamics). The first approach is an analytical formulation concerning a finite baffled cylinder and the second one is a numerical modelling for any type of shell of revolution.

The analytical formulation of a finite baffled cylinder immersed in a compressible (or incompressible) unbounded fluid domain is based on the usual method, which consists of expanding the displacements of the immersed shell in terms of the modal basis of the dry structure.

In this analytical study, unlike other studies, we do not use a boundary integral representation of the fluid, but we directly work with the fluid equation of motion. A parametric study shows that, depending on the information needed (i.e., the vibrating amplitude of the wall or the radiated pressure in the far field), the intermodal coupling due to the fluid has to be described with a different accuracy. Then, the dimension of the truncated modal basis has to be adapted. We also demonstrate that it is actually very difficult to predict the optimal dimension of the modal basis which will give a good accuracy on the vibrating amplitude of the wall.

The determination of the radiated pressure in the far field by the shell only requires a few terms in the development of the displacement in Fourier series. The mode shapes associated with the weak circumferential and longitudinal orders, have a preponderant influence compared to the large modes which can be neglected.

The analytical development is used as a reference in order to validate different numerical models. The numerical models presented in this paper are adapted to the solution of shell of revolution immersed in a fluid. Indeed, they couple the finite element method which is used for studying the shell, with the boundary element method which is used for studying the shell, with the boundary element method which is used for the analysis of the fluid.

One usual conical ring finite element is developed in order to discretize the axisymmetric shell. It makes it possible to determine the symmetric and antisymmetric motions of any shell of revolution with a small number of degrees of freedom.

Two discretizations of the boundary element integral are proposed. The first one, which is general, consists of modelling of the interface with planar panel elements which support constant densities of sources and normal dipoles. This model, coupling a conical ring finite element and a plane panel boundary element, is adapted to the study of an axisymmetric shell, which, for example, can be connected with a shell of any geometry and immersed in fluid. With a good accuracy, this model saves CPU time and requires less storage memory than the general model which couples a general shell finite element with a plane panel boundary element.

The second discretization, which is an original development is restricted only to the study of shells of revolution, and consists in using ring boundary elements for the discretization of the fluids/structure interface. In this case, the singularity distributions are developed in Fourier series. This model which couples ring finite elements and ring boundary elements is a substantial progress in the study of the behavior of submerged shells of revolution. Then, the coupled problem is completely defined by only one meridian line of the axisymmetric shell. With such a formulation, meshing the entire shell with shell or plate elements becomes useless.

Furthermore, it is unnecessary to mesh the fluid-structure interface by the classical collocation method using triangular or quadrilateral plane panels (Bérot & Peseux 1996; Sayhi *et al*. 1981). The dimensions of the fluid problem (90) are only equal to the number of ring boundary elements.

Finally, this new model allows us to significantly reduce the dimensions of the coupled problem, and as a consequence, the CPU time and the storage memory are drastically decreased. In the future, this model can be completed by axial or longitudinal stiffeners and will be easily used for the study of passive or active control processes. For example, the geometrical characteristics of the shell and the position of the acoustic sources can be optimized in order to reduce the radiated pressure in the far field.

ACKNOWLEDGEMENTS

We are grateful to Mr Michel Labrosse, graduate student at ECN, for giving us his help in the writing of this paper.

References

Beer, G. & Watson, J. O. 1992 *Introduction to Finite and Boundary Element Methods for Engineers*. New York: Wiley.

Bérot, F. 1997 Comportement hydroélastique et vibroacoustique de coque de révolution: formulations analytiques et modèles numériques. Thèse de Doctorat, Ecole Centrale de Nantes, France.

Bérot, F. & Peseux, B. 1996 Vibro-acoustic behaviour of cylindrical thin shells. Analytical formulation and numerical model. In *Fluid–Structure Interaction-1996* (eds C. Y. Wang, D. C. Ma, Y. W. Shin, R. F. Kulak, F. C. Chang, D. Bronchard, F. J. Moody & S. Kaneko), PVP-Vol. 337, pp. 129–139. New York: ASME.

Bérot, F. & Peseux, B. 1997 Dynamic behavior of submerged shells of revolution: Coupling of a ring finite element and a ring boundary element. In *Advances in Analytical, Experimental and Computational Technologies in Fluids, Structures, Transients and Natural Hazards* (ed. K. Karim-Panahi), PVP-Vol. 355, pp. 261–270. New York: ASME.

Brebbia, C. A. & Dominguez, J. 1992 *Boundary Element – An Introduction Course*, 2nd edition New York: McGraw-Hill.

Delhommeau, G. 1987 Les problèmes de diffraction-radiation et de résistance de vagues: étude théorique et résolution numérique par la méthode des singularités. Thèse de Doctorat es Sciences, ENSM Nantes, France.

Delhommeau, G., Peseux, B. & Quevat, J. P. 1981 Natural frequencies of immersed plates evaluated by mixed method finite element, boundary element. *Proceedings of the International Conference of Numerical Methods for Coupled Problems* pp. 346–355, Swansea, U.K.

Dym, C. L. 1973 Some new results for the vibrations of circular cylinders. *Journal of Sound and Vibration* **29,** 189–205.

Forsberg, K. 1964 Influence of boundary conditions on the modal characteristics of thin cylindrical shells. *AIAA Journal* **2,** 2150–2156.

Gonçalves, P. B. & Ramos, N. R. S. S. 1997 Numerical method for vibration analysis of cylindrical shells. *ASCE Journal of Engineering Mechanics* **123,** 544–550.

Gould, P. L. 1985 *Finite Element Analysis of Shells of Revolution*. London: Pitman Publishing Ltd.

Gould, P. L. & Basu, P. K. 1977 Geometric stiffness matrices for the finite element analysis of rotational shell. *Journal of Structural Mechanics* **5,** 87–105.

Grafton, P. E. & Strome, D. R. 1963 Analysis of axisymmetrical shells by direct stiffness method. *AIAA Journal* **1,** 2342–2347

Grosh, K., Pinsky, P. M., Malhotra, M. & Rao, V. S. 1994 Finite element formulation for baffled fluid-loaded, finite cylindrical shell. *International Journal for Numerical Methods in Engineering* **37,** 2971–2985.

Hall, W. S. 1994 *The Boundary Element Method*. Dordrecht: Kluwer Academic Publishers.

Hayeck, S. 1966 Vibration of a spherical shell in an acoustic medium. *Journal of the Acoustical Society of America* **40,** 342–348.

Junger, M. C. & Feit, D. 1972 *Sound, Structures, and their Interaction*, Cambridge, MA: MIT.

Lakis, A. A. & Païdoussis, M. P. 1971 Free vibration of cylindrical shells partially filled with liquid. *Journal of Sound and Vibration* **19,** 1–15.

Lakis, A. A. & Païdoussis, M. P. 1972 Prediction of the response of a cylindrical shell to arbitrary or boundary-layer-induced random pressure fields. *Journal of Sound and Vibration*, **25,** 1–27.

Lakis, A. A. & Neagu, S. 1997 Free surface effects on the dynamics of cylindrical shells partially filled with liquid. In *Proceedings of 4th International Symposium on Fluid–Structure Interactions, Aeroelasticity, Flow-Induced Vibration and Noise* (eds M. P. Païdoussis, M. K. Au-Yang, W. J. Bryan, S. S. Chen, Y. A. Hassan, F. J. Moody, S. J. Price, D. S. Weaver & S. Ziada), AD-Vol. 53-2, pp. 101–110, New York: ASME.

Laulagnet, B. & Guyader, J. L. 1989 Modal analysis of a shell's acoustic radiation in light and heavy fluids. *Journal of Sound and Vibration* **131,** 397–415.

Laulagnet, B. & Guyader, J. L. 1990 Sound radiation by finite cylindrical ring stiffened shell. *Journal of Sound and Vibration* **138,** 173–191.

Leissa, W. 1973 *Vibration of shells* NASA SP 288. Washington, DC: Scientific and Technical Information Office.

Lesueur, C. 1988 *Rayonnement acoustique des structures. Vibroacoustique, Interactions fluide–structure*. Paris: Editions Eyrolles.

Lindholm, U. S., Kaña, D. D. & Abramson, H. N. 1962 Breathing vibrations of a circular cylindrical shell with an internal liquid. *Journal of Aeronautical Science* **29,** 1052–1059.

Mistry, J. & Menezes, J. C. 1995 Vibration of cylinders partially-filled with liquids. *ASME Journal of Vibration and Acoustics* **117,** 87–93.

Morand, H. J. P. & Ohayon, R. 1995 *Fluid–Structure Interaction, Applied Numerical Methods*. New York: Wiley.

Naghdi, P. M. & Kalnins, A. 1962 On vibrations of elastic spherical shells. *Journal of Applied Mechanics* **29,** 65–72.

Oudin, H., Peseux, B. & Quevat, J. P. 1984 Dynamic Response of Coupled Problems. *Proceedings of International Conference of Numerical Methods for Coupled Problems*, pp. 340–347, Venise, Italy.

Percy, J. H., Pian, T. H. H., Klein, S. & Navaranta, D. R. 1965 Application of matrix displacement method to linear analysis of shell of revolution. *AIAA Journal* **3,** 2138–2145.

Peseux, B. 1989 Contribution à l'étude de structures partiellement ou totalement immergées en matériau homogène ou en composite. Thèse de Doctorat es Sciences, ENSM Nantes, France

Peseux, B. & Quevat, J. P. 1985 Linear fluid-structure interaction in unbounded domains. In *Fluid-Structure Dynamics* (eds S. J. Brown, D. C. Ma, W. K. Liu, C. Y. Wang, T. B. Belytschko, K. Karim-Panahi, S. S. Chen, F. J. Moody & Y. W. Shin), PVP-Vol. 98-7, pp. 185–188. New York: ASME.

Sandman, B. E. 1976 Fluid loading influence coefficients for a finite cylindrical shell. *Journal of the Acoustical Society of America* **60,** 1256–1264.

Sayhi, M. N., Ousset, Y. & Verchery, G. 1981 Solution of radiation problems by collocation of integral formulation in terms of single and double layer. *Journal of Sound and Vibration* **54,** 473–500.

Stepanishen, P. R. 1982 Modal coupling in the vibration of fluid-loaded cylindrical shells. *Journal of the Acoustical Society of America* **71,** 813–823.

Susbielle, G. & Bratu, C. H. 1981 *Vagues et Ouvrages Pétroliers en Mer*. Paris: Editions Technip.
Terhune, J. H. & Karim-Panahi, K. 1993 Wave motion of a compressible viscous fluid contained in a cylindrical shell. *ASME Journal of Pressure Vessel Technology* **115,** 302–312.
Wielgosz, C. 1976 Contribution à l'étude des vibrations des sphères et calottes sphériques de faible épaisseur. Thèse de Docteur Ingénieur, ENSM Nantes.
Zienkiewicz, O. C. & Taylor, R. L. 1991 *The Finite Element Method*, 4th Editon, Vol. I. London: McGraw-Hill.

APPENDIX A: ANALYTICAL FORMULATION

A.1. Flügge's and Donnell's Operators

Flügge's operator is expressed with respect to the displacement field of the mid-surface of the circular cylindrical shell by

$$[K] = \frac{Eh}{R^2(1-v^2)}\begin{bmatrix} 1+\eta+2\eta_{,\theta\theta}+\eta\nabla^4 & {}_{,\theta}-\eta R^2\left(\frac{3-v}{2}\right)_{,zz\theta} & vR_{,z}+\eta R\left(\frac{1-v}{2}\right)_{,\theta\theta z}-\eta R^3{}_{,zzz} \\ & R^2\left(\frac{1-v}{2}\right)(1+3\eta)_{,zz}+{}_{,\theta\theta} & R\left(\frac{1+v}{2}\right)_{,\theta z} \\ \text{sym} & & R^2{}_{,zz}+\left(\frac{1-v}{2}\right)(1+\eta)_{,\theta} \end{bmatrix},$$

where $\eta = \frac{1}{12}(h/R)^2$. Donnell's operator is obtained from Flügge's by neglecting the thickness h in comparison to the mean radius R; thus,

$$[K] = \frac{Eh}{R^2(1-v^2)}\begin{bmatrix} 1+\eta\nabla^4 & {}_{,\theta} & vR_{,z} \\ & R^2\left(\frac{1-v}{2}\right)_{,zz}+{}_{,\theta\theta} & R\left(\frac{1+v}{2}\right)_{,\theta z} \\ \text{sym} & & R^2{}_{,zz}+\left(\frac{1-v}{2}\right)_{,\theta\theta} \end{bmatrix},$$

with

$$\nabla^4 u = \Delta^2 u = u_{,\theta\theta\theta\theta} + 2R^2 u_{,\theta\theta zz} + R^4 u_{,zzzz}.$$

A.2. Coefficients of the Sixth-Order Equation (5)

The coefficients of the sixth-order equation, whose roots are the natural pulsations of the dry elastic shell are solutions, are defined as

$$A_1 = 1+\eta-2\eta n^2+\eta(n^2+\lambda^2)^2, \qquad B_2 = \left(\frac{1-v}{2}\right)(1+3\eta)\lambda^2+n^2,$$

$$B_1 = A_2 = -n-\eta\left(\frac{3-v}{2}\right)n\lambda^2, \qquad C_2 = B_3 = \left(\frac{1+v}{2}\right)n\lambda,$$

$$C_1 = A_3 = v\lambda-\eta\left(\frac{1-v}{2}\right)n^2\lambda+\eta\lambda^3, \qquad C_3 = \lambda^2+\left(\frac{1-v}{2}\right)(1+\eta)n^2.$$

If the governing equations of the dry circular cylindrical thin shell are derived from Flügge's theory, these coefficients must be used. In the case of Donnell's theory, they become

$$A_{1d} = 1 + \eta - 2\eta n^2 + \eta(n^2 + \lambda^2)^2, \qquad B_{2d} = \left(\frac{1-\nu}{2}\right)\lambda^2 + n^2,$$

$$B_{1d} = A_{2d} = -n, \qquad C_{2d} = B_{3d} = \left(\frac{1+\nu}{2}\right)n\lambda,$$

$$C_{1d} = A_{3d} = \nu\lambda, \qquad C_{3d} = \lambda^2 + \left(\frac{1-\nu}{2}\right)n^2,$$

with

$$\lambda = Rk_m \quad \text{and} \quad \eta = \frac{h^2}{12R^2}.$$

APPENDIX B: NUMERICAL MODEL

B.1. Stress-Strain Relationship

For an isotropic and homogeneous material, the stress-strain relationship used in the numerical model is defined as

$$\begin{Bmatrix} \sigma_s \\ \sigma_\theta \\ \sigma_{s\theta} \\ \tau_s \\ \tau_\theta \\ \tau_{s\theta} \end{Bmatrix} = \frac{Eh}{1-\nu^2} \begin{bmatrix} 1 & \nu & 0 & 0 & 0 & 0 \\ \nu & 1 & 0 & 0 & 0 & 0 \\ 0 & 0 & \dfrac{1-\nu}{2} & 0 & 0 & 0 \\ 0 & 0 & 0 & \dfrac{h^2}{12} & \dfrac{\nu h^2}{12} & 0 \\ 0 & 0 & 0 & \dfrac{\nu h^2}{12} & \dfrac{h^2}{2} & 0 \\ 0 & 0 & 0 & 0 & 0 & \dfrac{h^2(1-\nu)}{24} \end{bmatrix} \begin{Bmatrix} \varepsilon_s \\ \varepsilon_\theta \\ \varepsilon_{s\theta} \\ \chi_s \\ \chi_\theta \\ \chi_{s\theta} \end{Bmatrix}.$$

B.2. Coefficients of the Matrix $[\Pi_n^\delta]$

The coefficients of the matrix of meridian terms $[\Pi_n^\delta]$, equation (48), are expressed for the two symmetries of the displacement field, as follows:

$$\Pi_n^\delta(1,1) = \Pi_n^\delta(1,2) = \Pi_n^\delta(1,4) = \Pi_n^\delta(1,5) = \Pi_n^\delta(1,6) = \Pi_n^\delta(1,8) = 0,$$

$$\Pi_n^\delta(3,1) = \Pi_n^\delta(3,4) = \Pi_n^\delta(3,5) = \Pi_n^\delta(3,8) = 0,$$

$$\Pi_n^\delta(1,3) = \frac{2}{l_{ij}} N^w_{1,\xi}, \qquad \Pi_n^\delta(4,5) = -\frac{4}{l_{ij}^2} N^u_{3,\xi\xi},$$

$$\Pi_n^\delta(1,7) = \frac{2}{l_{ij}} N^w_{2,\xi}, \qquad \Pi_n^\delta(4,8) = -\frac{4}{l_{ij}^2} N^u_{4,\xi\xi},$$

$$\Pi_n^\delta(2,1) = \frac{1}{r} N^u_1 \cos\varphi, \qquad \Pi_n^\delta(5,1) = \frac{n^2}{r^2} N^u_1 - \frac{2}{r l_{ij}} N^u_{1,\xi} \sin\varphi,$$

$$\Pi_n^\delta(2,2) = \frac{(-1+2\delta)n}{r} N_1^v, \qquad \Pi_n^\delta(5,2) = \frac{(-1+2\delta)n}{r^2} N_1^v \cos\varphi,$$

$$\Pi_n^\delta(2,3) = -\frac{1}{r} N_1^w \sin\varphi, \qquad \Pi_n^\delta(5,4) = \frac{n^2}{r^2} N_2^u - \frac{2}{r l_{ij}} N_{2,\xi}^u \sin\varphi,$$

$$\Pi_n^\delta(2,4) = \frac{1}{r} N_2^u \cos\varphi, \qquad \Pi_n^\delta(5,5) = \frac{n^2}{r^2} N_3^u - \frac{2}{r l_{ij}} N_{3,\xi}^u \sin\varphi,$$

$$\Pi_n^\delta(2,5) = \frac{1}{r} N_3^u \cos\varphi,$$

$$\Pi_n^\delta(2,6) = \frac{(-1+2\delta)n}{r} N_2^v, \qquad \Pi_n^\delta(5,6) = \frac{(-1+2\delta)n}{r^2} N_2^v \cos\varphi,$$

$$\Pi_n^\delta(2,7) = -\frac{1}{r} N_2^w \sin\varphi, \qquad \Pi_n^\delta(5,8) = \frac{n^2}{r^2} N_4^u - \frac{2}{r l_{ij}} N_{4,\xi}^u \sin\varphi,$$

$$\Pi_n^\delta(2,8) = \frac{1}{r} N_4^u \cos\varphi, \qquad \Pi_n^\delta(6,1) = 2\frac{(-1+2\delta)n}{r l_{ij}} N_{1,\xi}^u - \frac{(-1+2\delta)n}{r^2} N_1^u \sin\varphi,$$

$$\Pi_n^\delta(3,2) = \frac{1}{l_{ij}} N_{1,\xi}^v + \frac{1}{2r} N_1^v \sin\varphi, \qquad \Pi_n^\delta(6,2) = \frac{2}{r l_{ij}} N_{1,\xi}^v \cos\varphi - \frac{1}{r^2} N_1^v \sin\varphi\cos\varphi,$$

$$\Pi_n^\delta(3,3) = -\frac{(-1+2\delta)n}{2r} N_1^w, \qquad \Pi_n^\delta(6,4) = 2\frac{(-1+2\delta)n}{r l_{ij}} N_{2,\xi}^u - \frac{(-1+2\delta)n}{r^2} N_2^u \sin\varphi,$$

$$\Pi_n^\delta(3,6) = \frac{1}{l_{ij}} N_{2,\xi}^v + \frac{1}{2r} N_2^v \sin\varphi, \qquad \Pi_n^\delta(6,5) = 2\frac{(-1+2\delta)n}{r l_{ij}} N_{3,\xi}^u - \frac{(-1+2\delta)n}{r^2} N_3^u \sin\varphi,$$

$$\Pi_n^\delta(3,7) = -\frac{(-1+2\delta)n}{2r} N_2^w, \qquad \Pi_n^\delta(6,6) = \frac{2}{r l_{ij}} N_{2,\xi}^v \cos\varphi - \frac{1}{r^2} N_2^v \sin\varphi\cos\varphi,$$

$$\Pi_n^\delta(4,1) = -\frac{4}{l_{ij}^2} N_{1,\xi\xi}^u, \qquad \Pi_n^\delta(6,8) = 2\frac{(-1+2\delta)n}{r l_{ij}} N_{4,\xi}^u - \frac{(-1+2\delta)n}{r^2} N_4^u \sin\varphi,$$

$$\Pi_n^\delta(4,4) = -\frac{4}{l_{ij}^2} N_{2,\xi\xi}^u;$$

APPENDIX C: ANALYTICAL VALUES

C.1. Analytical Eigenfrequencies of a Dry Cylindrical Shell (Flügge's Theory)

The mechanical characteristics of the cylinder are: Young's modulus $E = 2 \times 10^{11}$ N/m^2, Poisson's ratio $v = 0{\cdot}3$, density $\rho_s = 7850$ kg/m^3. The geometrical characteristics are: length $L = 1{\cdot}2$ m, mean radius $R = 0{\cdot}4$ m, thickness $h = 0{\cdot}003$ m (Table C1).

C.2. Analytical Eigenfrequencies of a Cylindrical Shell Immersed in Water (Flügge's Theory)

The mechanical characteristics of the cylinder are: Young's modulus $E = 2 \times 10^{11}$ N/m^2, Poisson's ratio $v = 0{\cdot}3$, density $\rho_s = 7850$ kg/m^3. The geometrical characteristics are: length $L = 1{\cdot}2$ m, mean radius $R = 0{\cdot}4$ m, thickness $h = 0{\cdot}003$ m. The water density is $\rho_f = 1000$ kg/m^3 (Table C2).

TABLE C1

Eigenfrequencies (in Hz) of a dry simply supported cylindrical shell by Flügge's theory

m	n	$i=1$	$i=2$	$i=3$	m	n	$i=1$	$i=2$	$i=3$
1	0	566·4	1304·3	2212·4	2	0	724·9	2608·6	4415·5
1	1	310·6	1843·0	3076·4	2	1	601·3	2913·9	4898·1
1	2	149·7	2834·3	4794·8	2	2	411·9	3640·9	6120·2
1	3	88·1	3969·6	6735·1	2	3	281·0	4584·5	7734·6
1	4	65·4	5157·0	8750·9	2	4	202·8	5643·5	9542·0
1	5	68·1	6367·3	10800·0	2	5	160·6	6766·1	11451·0
1	6	89·6	7589·2	12866·7	2	6	147·2	7925·7	13418·2
1	7	123·4	8817·0	14943·7	2	7	158·9	9108·3	15421·5
1	8	166·5	10050·9	17027·3	2	8	190·3	10306·0	17448·4
1	9	218·2	11286·7	19115·4	2	9	236·0	11513·9	19491·6

m	n	$i=1$	$i=2$	$i=3$	m	n	$i=1$	$i=2$	$i=3$
3	0	840·4	3912·9	6619·5	4	0	932·4	5217·3	8823·7
3	1	771·3	4118·1	6948·8	4	1	888·2	5370·5	9072·8
3	2	625·1	4665·5	7854·6	4	2	780·7	5800·3	9782·1
3	3	483·5	5441·0	9166·4	4	3	655·1	6443·9	10861·8
3	4	375·0	6362·3	10734·7	4	4	541·3	7242·2	12213·2
3	5	300·4	7377·3	12462·3	4	5	450·7	8150·5	13755·8
3	6	255·6	8453·4	14291·2	4	6	385·8	9137·0	15432·0
3	7	238·6	9570·7	16187·0	4	7	347·0	10179·9	17202·6
3	8	247·3	10716·3	18128·8	4	8	334·3	11263·7	19041·2
3	9	278·0	11882·2	20103·2	4	9	346·5	12378·0	20929·8

m	n	$i=1$	$i=2$	$i=3$
5	0	1009·2	6521·6	11028·1
5	1	978·5	6643·6	11228·0
5	2	897·9	6994·3	11807·8
5	3	793·2	7537·4	12715·4
5	4	687·2	8232·4	13886·6
5	5	593·6	9043·8	15260·3
5	6	519·2	9943·6	16786·5
5	7	467·0	10910·5	18427·3
5	8	438·9	11928·6	20154·4
5	9	435·4	12986·1	21947·5

TABLE C2

Eigenfrequencies (in Hz) of a simply supported cylindrical shell immersed in water by Flügge's theory

m	n	$i=1$	$i=2$	$i=3$	m	n	$i=1$	$i=2$	$i=3$
1	0	1799·4	1304·3	2460·8	2	0	1983·1	2608·3	4465·7
1	1	784·7	2147·0	3428·3	2	1	1498·5	3092·4	4985·6
1	2	382·7	2961·9	5100·1	2	2	968·6	3815·0	6254·6
1	3	209·5	4024·3	6972·1	2	3	626·4	4697·7	7878·9
1	4	143·4	5183·4	8936·0	2	4	426·6	5711·8	9675·8
1	5	139·1	6381·4	10948·1	2	5	319·3	6807·8	11569·0
1	6	172·4	7597·4	12987·9	2	6	278·1	7952·1	13520·9
1	7	225·6	8823·1	15045·0	2	7	286·9	9125·7	15510·7
1	8	291·7	10054·3	17113·3	2	8	330·1	10317·8	17526·2
1	9	368·3	11289·0	19189·5	2	9	395·5	11522·2	19560·0

TABLE C2 (continued)

m	n	$i=1$	$i=2$	$i=3$	m	n	$i=1$	$i=2$	$i=3$
3	0	1998·0	3913·0	6647·2	4	0	2004·5	5217·3	8842·6
3	1	1779·4	4181·9	6987·4	4	1	1884·1	5397·1	9095·9
3	2	1374·1	4782·5	7916·3	4	2	1607·1	5867·6	9816·1
3	3	1015·6	5552·0	9246·3	4	3	1302·8	6257·5	10908·1
3	4	753·0	6446·6	10821·5	4	4	1039·1	7230·7	12268·4
3	5	577·0	7438·2	12547·8	4	5	835·1	8215·6	13815·2
3	6	470·8	8496·2	14371·5	4	6	690·7	9188·1	15491·9
3	7	422·7	9600·9	16260·6	4	7	601·3	10218·9	17260·6
3	8	423·1	10738·0	18195·5	4	8	562·0	11293·5	19096·1
3	9	460·7	11898·1	20163·5	4	9	566·4	12400·8	20981·1

m	n	$i=1$	$i=2$	$i=3$
5	0	2008·7	6521·6	11042·2
5	1	1933·2	6656·7	11244·2
5	2	1740·9	7033·2	11829·6
5	3	1500·2	7595·0	12744·7
5	4	1264·6	8295·5	13922·8
5	5	1062·1	9103·1	15301·5
5	6	903·2	9994·9	16830·5
5	7	790·5	10952·9	18471·9
5	8	723·8	11962·9	20198·4
5	9	700·5	13013·7	21990·0